0 0 0 0 4 4 0 0 0 1 3

LBL-4312
c.1

K VACANCY PRODUCTION IN MEDIUM-Z HEAVY ION COLLISIONS

R. Anholt
(Ph.D thesis)

December 1975

Prepared for the U. S. Energy Research and Development Administration under Contract W-7405-ENG-48

For Reference

Not to be taken from this room

LAWRENCE BERKELEY LABORATORY
UNIVERSITY OF CALIFORNIA
BERKELEY

LBL-4312
c.1

DISCLAIMER

This document was prepared as an account of work sponsored by the United States Government. While this document is believed to contain correct information, neither the United States Government nor any agency thereof, nor the Regents of the University of California, nor any of their employees, makes any warranty, express or implied, or assumes any legal responsibility for the accuracy, completeness, or usefulness of any information, apparatus, product, or process disclosed, or represents that its use would not infringe privately owned rights. Reference herein to any specific commercial product, process, or service by its trade name, trademark, manufacturer, or otherwise, does not necessarily constitute or imply its endorsement, recommendation, or favoring by the United States Government or any agency thereof, or the Regents of the University of California. The views and opinions of authors expressed herein do not necessarily state or reflect those of the United States Government or any agency thereof or the Regents of the University of California.

0 0 0 0 4 4 0 3 3 1 4

TABLE OF CONTENTS

ABSTRACT vii

I. INTRODUCTION 1

II. THEORETICAL METHODS 7

2.1 Plane Wave Born Approximation 7

2.2 Semi-Classical Approximation 9

2.3 Binary Encounter Approximation 11

2.4 Perturbed Stationary States Method 15

III. EXPERIMENT 26

IV. EXPERIMENTAL RESULTS 34

4.1 Basic Relations 34

4.2 Thick Target Yield Data 38

4.3 Scaling Laws 43

V. THEORY OF 1sσ EXCITATION 56

5.1 Model Calculations for p + H Collisions 56

5.1.1 The total cross section 58

5.1.2 P(b,E) 62

5.1.3 The differential cross section 64

5.2 The Binding Energy Correction 66

5.3 Comparison 70

5.4 Excitation to High Bound States 74

VI. EXPERIMENT AND THEORY 77

6.1 The Data 77

6.2 Other Corrections 83

6.2.1 Polarization 83

6.2.2 Charge exchange and Demkov coupling 89

6.3 Conclusions 91

VII. CONCLUSIONS 93

REFERENCES 98

APPENDIX A: On 1sσ Thick Target Yield Data 102

APPENDIX B: Theory of 1sσ Ionization: Model Calculations 106

APPENDIX C: Excitation to High Bound States 119

APPENDIX D: The Development of the Binding Factor 121

ACKNOWLEDGMENTS

In doing this work, I had the good fortune of having W. E. Meyerhof of Stanford University as a collaborator. This has been a very fruitful collaboration; little of this work would have been possible without his considerable interest and devotion to this subject. I also thank him for reading this thesis and for providing many valuable suggestions.

I would like to thank my research advisor, John Rasmussen, for supporting this work. I also greatly benefitted from working with F. S. Stephens, R. M. Diamond, and their group. They provided much of the equipment used in our experiments.

Others deserving thanks are Richard Eggers, David Raich, and Richard Leres whom I conned many a time into writing computer magnetic tape translation sub-programs for me. The accelerator crews at the SuperHILAC and the Stanford tandem have been very helpful. I would also like to thank T. K. Saylor who collaborated closely on many projects at Stanford.

In doing the theoretical calculations described in Chapter V I acknowledge the help of Walter Thorson (University of Alberta). Much of the data described in Chapter VI was kindly supplied by Tom Gray and F. D. McDaniel. The Br and I data discussed throughout this thesis was taken by W. E. Meyerhof, T. K. Saylor, S. M. Lazarus, A. D. Little, B. B. Triplett, and L. Chase, Jr..

Finally one of the advantages of working at the Lawrence Berkeley Laboratory is the number of highly qualified engineers, electronic designers, machinists, technicians, and other scientists

whom I have been able to consult. By freely sharing their experiences with me, they provided an invaluable technical education (not to mention services). Some of these people are Don Landis, Joe Jaklevic, Norm Madden, Harry Bowman, Dick Escobales, Gordon Steers, Dick Pehl, Leon Archambault, G. G. Young, George Gabor, Hans Krapf, Mon Lee, Chuck Corum, and Dave. Ward.

This work was done under the auspices of the U. S. Energy Research and Development Administration.

0 0 0 0 4 4 0 3 3 1 6

K VACANCY PRODUCTION IN MEDIUM-Z HEAVY ION COLLISIONS

R. Anholt

Lawrence Berkeley Laboratory
University of California
Berkeley, California 94720

Ph.D. Thesis
December 1975

ABSTRACT

During slow encounters between projectile and target atoms, the electronic atomic wavefunctions of the two collision partners distort and form Molecular Orbitals (MOs). This thesis considers K vacancy formation in slow heavy-ion collisions which occur when electrons are excited out of the 2pσ and 1sσ MOs.

Experimental work using 200 MeV Kr ions is described. Thick target yields of projectile and target K x rays coming from 2pσ and 1sσ excitation are identified.

Our main interest is the excitation of electrons from the 1sσ MO. This cannot be observed in symmetric or near symmetric collisions since Demkov coupling between the projectile and target K shells at large internuclear distances cause vacancies, which are created in the 2pσ orbital, to be transferred into the 1sσ orbital giving an apparent 1sσ yield many orders of magnitude larger than for direct excitation. In collisions

involving Kr ions, 1sσ vacancy production is only observed in very asymmetric collisions: as Kr K x rays in encounters with target atoms between H and Ar, and as target K x rays in encounters with atoms between Ce and U.

Theoretical approximate calculations of 1sσ ionization cross sections are described. The calculations indicate that when the experimental proton $+Z_2$ cross section (σ_p) is known (where Z_2 is the target atomic number), the $Z_1 + Z_2$ cross section can be calculated from the relation:

$$\sigma(v_1) = \sigma_p(v_1) Z_1^2 \left[\frac{U_K(Z = Z_2 + 1)}{U_K(Z = Z_1 + Z_2)} \right]^n$$

where Z_1 ($<Z_2$) is the projectile atomic number, U_K is the K binding energy, and n is a constant depending on the reduced projectile velocity v_1/v_K (v_K is the velocity of the K-shell electron). This formula may also be used where $Z_2 < Z_1$ by interchanging Z_1 and Z_2 everywhere.

Data from experiments where the target K vacancy cross section is measured as a function of the projectile charge (at the same velocity) are discussed. The above relationship fits the data but n is not as large as theory indicates. Finally we compare our Kr data and other heavy ion data with this relation.

I. INTRODUCTION

K vacancy or K x ray production in particle-atom collisions has usually been studied with light projectile ions: electrons, protons, and alpha particles. Generally K vacancy production by these light particles is well understood; the overall agreement between experiment and theory is better than a factor of two.[1] Recently new effects such as polarization of the initial state,[2] contributions from distant collisions,[3] binding corrections,[4] and charge exchange between the target K shell and the projectile[5] have been discovered. These effects do suggest a need for improvement of the theory of K vacancy formation by light projectiles. Nevertheless, the agreement between theory and experiment is sufficiently close, so that theoretical cross sections can be used with fair confidence in many applications where K vacancy cross sections have yet to be measured.

With the development of medium high energy heavy ion accelerators it has become possible to examine K vacancy production in collisions where the projectile atomic number is nearly identical to the target atomic number. In these systems, the small disturbing effects which have been discovered in the light projectile data become overwhelmingly important, so that the light projectile theories are not applicable. Heavy ions introduce some totally new pathways for producing vacancies which do not contribute in light projectile-heavy target collisions and which are not simple extensions of polarization, distant collision, binding, and charge exchange effects. For instance in symmetric heavy ion collisions, there are strong coupling mechanisms for the formation of K vacancies, whereas in light projectile-heavy target collisions only weak coupling mechanisms are allowed. One must also consider K

vacancy production in the projectile as well as the target atom. K vacancy formation in light highly stripped projectiles was not previously considered since the projectile usually has no K electrons when it enters the target.

These new considerations have led to an examination of K vacancy formation in near symmetric heavy ion collisions from a new perspective. With light projectiles, only excitation out of the atomic K shell as a result of the perturbation by the Coulomb field of the projectile needs to be considered. Simple first order semi-classical time dependent perturbation theory can be used; in fact the problem can be solved very simply, but inexactly, and is an elementary quantum mechanics textbook problem.[6]

In symmetric heavy ion collisions the perspective taken is that excitation occurs from molecular orbitals (MOs) and not atomic orbitals.[7] This requires that the projectile velocity be sufficiently slow so that the electrons can adjust their motion to the presence of both the projectile and target nuclei. As long as this requirement is fulfilled, the electron has a wavefunction appropriate to a diatomic molecule with nuclear charges Z_1 and Z_2, the projectile and target atomic numbers respectively. The electronic energy levels will also correspond to the diatomic molecule. Figure 1 shows a plot of these energy levels as a function of internuclear distance R for a collision between two Ar atoms. We call this a correlation diagram.

Examination of diagrams such as this allows us to make some qualitative remarks about vacancy production in symmetric heavy ion collisions. For instance, Ar K vacancies can be formed mainly in two ways, from vacancy production in the $2p\sigma$ MO and from vacancy production

0 0 0 0 4 4 0 3 3 1 8

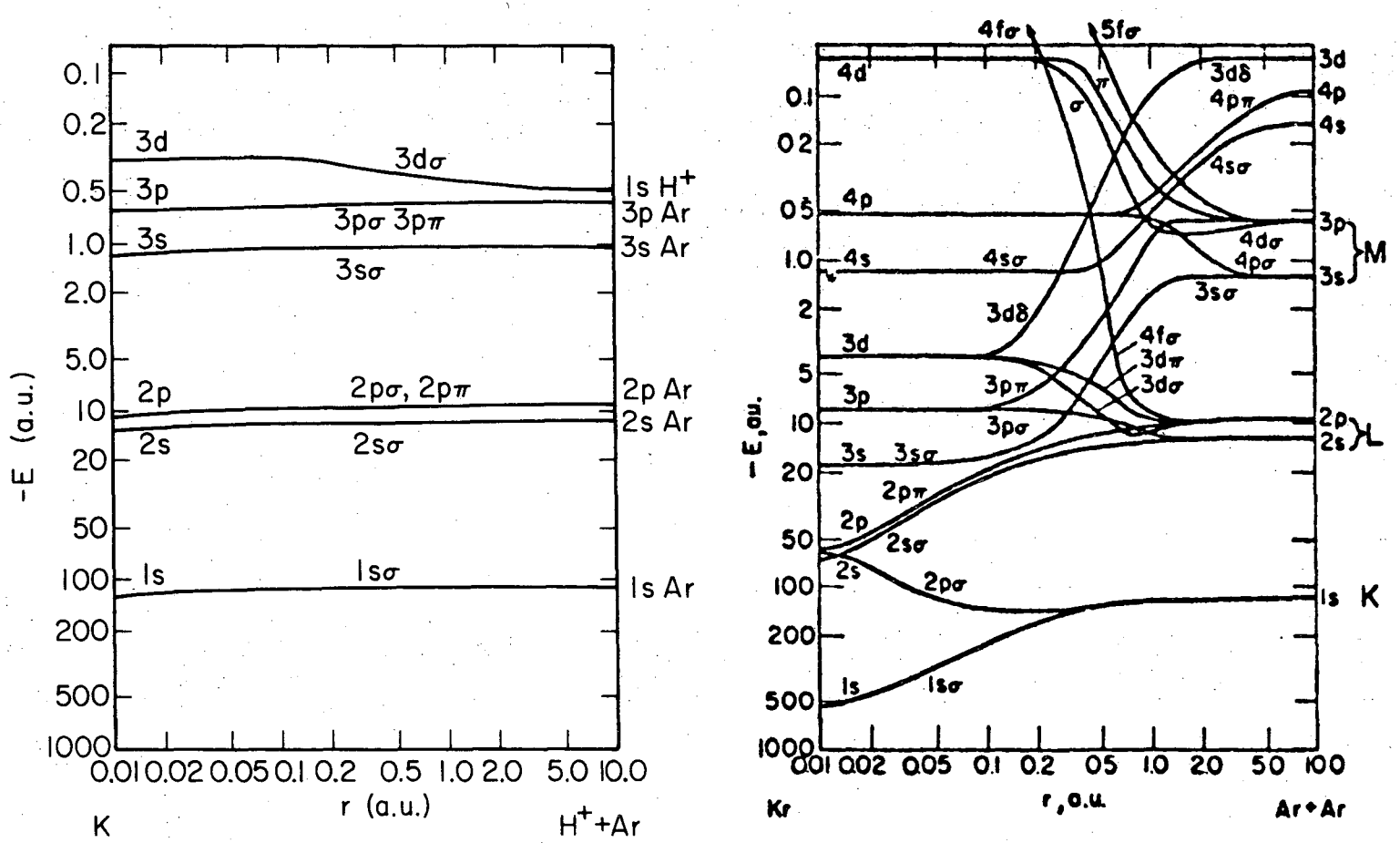

Fig. 1. Correlation diagram for H^+ + Ar and Ar + Ar collisions. Ar + Ar diagram taken from Lichten.[7] H^+ + Ar diagram is qualitative only. XBL 7511-9058

in the 1sσ MO. Both projectile and target atom vacancies are made, but in an exactly symmetric collision there is no way of determining whether an x ray comes from the target or projectile atom. Similarly there is no way of determining whether the vacancy was formed in the 1sσ or 2pσ MO. In light projectile collisions, e.g., p + Ar, for which a correlation diagram is also shown in Fig. 1, there is not a similar choice between vacancy production in the 2pσ or 1sσ orbitals; it must occur in the 1sσ orbital.

With the possibility of K vacancy production in the 2pσ orbital, new mechanisms for the formation of K vacancies can come into play. For instance if vacancies exist in the 2pπ MO, during a near head-on collision they correlate to the united atom (UA) $2p_{3/2}$ (or $2p_{\pm 1}$) level which strongly mixes with the $2p_{1/2}$ (or $2p_0$) level. On the outgoing part of the collision the vacancy may travel down the 2pσ orbital ending up as a K vacancy in either the projectile or target.[7] Coriolis coupling between the 2pσ and 2pπ levels is extremely strong, mostly because the energy levels are degenerate at the UA limit, and large cross sections for the formation of K vacancies result. Clearly no similar mechanism is available in the p + Ar collisions and the cross section there is comparatively small.

In certain situations, to be discussed below, one is interested in forming vacancies in the 1sσ orbital in symmetric collisions. The energy that the projectile must transfer to the 1sσ electron is approximately four times greater at the UA limit than the energy which must be transferred in proton induced collisions. In this case it turns out that the cross section can be smaller than in the proton collisions with the same projectile velocity.

There are more complex mechanisms for the formation of K vacancies in near symmetric heavy ion collisions. The purpose of this thesis is to examine the many possible pathways for K vacancy production, to determine which are most important, and ultimately to develop quantitative methods to predict these cross sections.

To delineate possible mechanisms of K vacancy formation we have measured K x ray cross sections and thick target yields in a variety of systems. Measurements using Kr ions at the Berkeley SuperHILAC are described in Chapter III of this thesis. The interpretation of the data is discussed in Chapter IV. Experiment tells us only what the yields are, using certain combinations of projectile and target atoms. To distinguish different mechanism for the formation of K vacancies we describe theoretical calculations, mostly for 1sσ ionization, in Chapter V. The theoretical calculations indicate that the 1sσ ionization cross section can be written as

$$\sigma = C Z^2 U_{UA}^{-n} \tag{1.1}$$

where C and n are projectile velocity dependent constants, Z is either the projectile atomic charge in collisions where target K vacancy cross sections are measured or the target atomic charge where projectile K vacancy cross sections are measured, and U_{UA} is the UA binding energy. In Chapter VI, this relation is compared with data obtained when the target K vacancy cross sections were measured as a function of the projectile charge Z_1, keeping the projectile velocity constant. The projectile velocity dependence of n is found. The value of n is never as large as theory indicates and possible reasons for this are

discussed. Finally we compare this relation with our Kr data and also Xe, I, and Br data in Chapter VII.

Although this thesis is concerned with K vacancy formation, which includes formation of vacancies in the 2pσ orbital as well as the 1sσ orbital, our interest is centered on K vacancy formation in the 1sσ orbital. For this reason, I shall have very little to say about the formation vacancies in the 2pσ MO. Since our interest is also restricted to medium-Z heavy ions, little will be said about the 2pσ - 2pπ rotational transition on which there is a copious amount of theoretical and experimental work.[8,9] A more complete summary of K vacancy production mechanisms is in preparation in collaboration with Meyerhof *et al.*[10] Recent reviews provide a summary of K vacancy production in ion-atom collisions with emphasis on light-Z heavy ion collisions,[11,12] and light projectile-heavy target collisions.[1,13]

II. THEORETICAL METHODS

Three major theories have been developed to explain K vacancy production in light projectile-heavy target collisions. These are Plane Wave Born[14] (PWBA), Binary Encounter (BEA),[1,15,16] and Semi-Classical (SCA) Approximations.[17] Although they are not, without drastic modifications, applicable in near symmetric heavy-ion collisions, I shall have occasion to refer to them, so it is appropriate to outline the way K vacancy cross sections are obtained by these approaches and to specify the limits of applicability of each model. We also introduce the only model which really is applicable in near symmetric heavy ion collisions: the Perturbed Stationary States (PSS) method.[18,19]

2.1 Plane Wave Born Approximation (PWBA)[13,14]

Cross sections for any elastic or inelastic collision process may be obtained in the first Born approximation by calculating the transition amplitude between specified initial and final states. K-shell ionization is an inelastic process where the perturbing potential $V(\vec{R},\vec{r})$ is the Coulomb field of the projectile. The transition amplitude is defined as:

$$T_{fi} = Z_1 e^2 \iint d^3\vec{R}\, d^3\vec{r}\; \Phi_f(\vec{R},\vec{r})\, \frac{1}{|\vec{R}-\vec{r}|}\, \Psi_i(\vec{R},\vec{r}) \qquad (2.1)$$

where $\vec{R}$ is the nuclear coordinate and $\vec{r}$ is the electron coordinate. In the PWBA theory, the initial and final wavefunctions, ψ_i and Φ_f, are approximated by products of eigenfunctions of the Hamiltonian of the target atom H_a, which depends only on electron coordinates, and eigenfunctions of the wave equation for the motion of the projectile nucleus H_p. Internal coordinates of the projectile atom are neglected and the

projectile wavefunction is taken to be a plane wave. It is usual to approximate the initial target atomic wavefunction by a screened hydrogenic 1s wavefunction with charge $Z_2^* = Z_2 - 0.3$. For the final state the ejected target electron is described by an outgoing Coulomb wave. In calculating the transition amplitude, the integral over nuclear coordinates is usually evaluated first. The problem is then reduced to calculating a single time independent matrix element. The cross section is obtained (non-relativistically) from:

$$d\sigma_f = \frac{(2\pi)^4}{v_1} |T_{fi}|^2 \, d^3\vec{K}_f \, \delta(E_f - E_i) \tag{2.2}$$

where $\vec{K}_f$ is the final momentum of the projectile, v_1 is the projectile velocity, and E_f and E_i are the final and initial projectile kinetic plus electron binding energies.

It is not our purpose to detail the procedures by which cross sections are obtained from these equations. Both the total cross section and the cross section differential in the final ejected electron energy ε may be obtained.[14] The cross sections obtained from the PWBA have the convenient property of being functions of only two variables, η_K and θ_K. The variable η_K is the square of the ratio of the projectile (LAB) velocity to the K electron velocity:

$$\eta_K = \left(\frac{v_1}{v_K}\right)^2 = \frac{E_1}{\lambda A_1 U_K} \tag{2.2a}$$

where E_1 and A_1 are the projectile energy and mass number, λ is the ratio of proton to electron mass, and U_K is K electron binding energy. The PWBA theory uses a simple Slater screening factor,[20] replacing Z_2 by $Z_2^* = Z_2 - 0.3$ to obtain the one-electron K shell wavefunction. The

variable θ_K is the ratio of the experimental binding energy to the idealized or "Slater rule" binding energy: $U_S = 0.0136\ Z_2^{*2}$ keV. In terms of these two variables the cross section can be written as:

$$\sigma = \frac{Z_1^2}{Z_2^{*4}} f(\eta_K, \theta_K)/\theta_K \tag{2.3}$$

where Z_1 and Z_2 will consistently be taken in this work as projectile and target atomic number respectively. Tabulations of the f function[21] are available so that cross sections may easily be obtained.

2.2 Semi-Classical Approximation (SCA)[17,22]

In the collisions of interest to us, the nuclei follow practically classical paths, Rutherford orbits. The nuclear collision can be specified by its impact parameter b, and the probability of forming a K vacancy along this path can be defined. Studies of the differential cross section as a function of b give more detailed information about K vacancy production than do total cross sections; also, a more detailed theory than the PWBA is needed to predict impact parameter probabilities. The SCA developed by Bang and Hansteen[17] is such a theory. Using this method, the amplitude for excitation of an electron from an initial to final state is calculated by performing a time integral along a projectile trajectory with specified impact parameter b and energy E_1:

$$a(\hbar\omega_f, b, E_1, \infty) = \int_{-\infty}^{\infty} dt \langle \Phi_f^a | V(t) | \Psi_i^a \rangle e^{i(\omega_f - \omega_i)t} \tag{2.4}$$

where $\hbar\omega_i$ and $\hbar\omega_f$ are the initial and final electron energies. The perturbing potential is the projectile's Coulomb field as in the PWBA theory. When K shell ionization is considered, the initial wavefunction

ψ_i^a is the atomic 1s wavefunction and the final wavefunction Φ_f^a is just the outgoing Coulomb wave for the ejected electron. The projectile nuclear eigenfunction (plane wave) is not included here. Since only the potential is a function of time, the integral over t is generally performed before evaluating the matrix element. In many applications, we will be interested in the cross section for ionization where $\hbar\omega_f$ is the energy of the ejected electron ε. Once the amplitude is obtained, the cross section for ionization is obtained by summing or integrating over final states and integrating over impact parameter

$$\sigma(E) = \int_0^\infty d\varepsilon \int_0^\infty 2\pi b db \, |a(\varepsilon, b, E, \infty)|^2 \tag{2.5}$$

Cross sections differential in final electron kinetic energy ε and the impact parameter dependence of the total K vacancy production probability may also be obtained:

$$\frac{d\sigma(\varepsilon, E)}{d\varepsilon} = \int_0^\infty 2\pi b db \, |a(\varepsilon, b, E, \infty)|^2 \tag{2.6}$$

$$P(b, E) = \int_0^\infty d\varepsilon \, |a(\varepsilon, b, E, \infty)|^2 \tag{2.7}$$

The total cross section has the same scaling properties as the cross section obtained in the PWBA theory. P(b,E) and $d\sigma/d\varepsilon$ have similar scaling properties:

$$\sigma(E) = \frac{Z_1^2}{Z_2^{*4}} f(n_K, \theta_K)/\theta_K$$

$$P(b, E) = \frac{Z_1^2}{Z_2^{*2}} g(n_K, B_K)/\theta_K \tag{2.8}$$

$$\frac{d\sigma(E, \varepsilon)}{d\varepsilon} = \frac{Z_1^2}{Z_2^{*6}} h(n_K, w, \theta_K)$$

where B_K is the ratio of the impact parameter to the target K shell radius b/a_K and $W = \varepsilon/U_K$. Tabulations of the f and g functions were recently published by Hansteen *et al.*[23] Differential cross sections have been calculated,[22] but tabulations of the h function are not available.

2.3 The Binary Encounter Approximation (BEA)[1,15,16]

The BEA theory is a classical theory. The ejection of a K shell electron into the continuum is viewed as the Rutherford scattering of the electron by the projectile with an energy transfer to the electron in excess of the K electron binding energy. We should keep in mind that the maximum energy transferred in Rutherford scattering collisions is[14]

$$E_m = \frac{2\mu}{(M+m)} \left(Mv_1 - mv_2\right)\left(v_1 + v_2\right) \tag{2.9}$$

where μ is the reduced mass between the projectile of mass M and the electron of mass m and v_2 and v_1 are the initial electron and projectile velocities. If the electron velocity v_2 could be neglected, K shell vacancy production would be a trivial problem.[3] However, for a 30 MeV Br projectile the maximum energy transferred to an electron at rest is only 0.8 keV which is insufficient to produce K vacancies in any element heavier than Na. In slow ion-atom collisions then, it is the initial electron motion within the atom when it strikes the projectile, which allows ionization to occur.

In Eq. (2.9) one can usually neglect the v_2^2 term which enters to order m_1/A_1M, where m_1 and A_1M are the electron and projectile masses. We can also neglect the v_1^2 term which is only of order 0.8 keV in our

example. The minimum initial electron kinetic energy E_2 required to give an energy transfer U_K is given by

$$U_K = \frac{2\mu}{M_1+m}(M-m)v_1v_2$$
$$\approx 4\left[E_1E_2/(\lambda A_1)\right]^{1/2} \tag{2.10}$$

For 30 MeV Br exciting Br, E_2 must be at least 56 keV, i.e. the Br K electron must be traveling at twice its average velocity v_K or with a kinetic energy equal to four times its average kinetic energy. Quantum mechanically the Br 1s electron has a probability $f(v_2)$ of having the required velocity v_2. This probability is given by the absolute square of the momentum wavefunction which is the Fourier transform of the K shell configuration wavefunction.[15] For a hydrogenic 1s electron:

$$f(v_2) = \frac{32}{\pi}\frac{v_2^2\, v_0^5}{(v_2^2+v_0^2)^4} \tag{2.11}$$

where $\frac{1}{2}mv_0^2$ is the idealized or "Slater rule" binding energy. The probability of the K electron traveling at twice its average velocity is not very large, and correspondingly the 1s ionization cross section will not be very large either. As E_1 decreases, the initial electron energy must be even greater so the probability $f(v_2)$ and thus the cross section will be even smaller.

To develop a classical theory, therefore, one must calculate the cross section for an electron of initial velocity and direction $\vec{v}_2$ Rutherford scattering from a projectile with initial velocity and direction $\vec{v}_1$ with an energy transfer ΔE. The average over the direction of $\vec{v}_1$ relative to $\vec{v}_2$, constrained to a specified energy transfer ΔE,

has been evaluated by Gerjuoy[24] and others,[25] so that a scattering cross section depending only on the scalar quantities ΔE, v_1, and v_2 is obtained. The total cross section for energy transfer ΔE by a projectile with velocity v_1 may then be obtained by averaging over the quantum mechanical velocity distribution $f(v_2)$:

$$\frac{d\sigma(\Delta E, v_1)}{d\Delta E} = \int_0^\infty f(v_2)\,dv_2\,\frac{d\sigma}{d\Delta E}(\Delta E, v_1, v_2) \tag{2.12}$$

The ionization cross section differential in final electron kinetic energy is

$$\frac{d\sigma}{d\varepsilon}(\varepsilon, E) = \frac{d\sigma}{d\Delta E}\left(\Delta E = U_K + \varepsilon, \sqrt{2E/M_1}\right) \tag{2.13}$$

and the total ionization cross section is

$$\sigma(E) = \int_0^\infty \frac{d\sigma}{d\varepsilon}\,d\varepsilon \tag{2.14}$$

As with the PWBA and SCA theories, scaling relationships exist and tabulations of $f(\eta_K, \theta_K)$ are available, but only, as far as I know, for $\theta_K = 1$.[1]

The impact parameter dependence of the probability for ionizing a K electron cannot be obtained in a straightforward manner but can be inferred by considering the integral over v_2. Classically, a velocity v_2 implies the electron must be orbiting at a distance from the target nucleus given by the Bohr atom relation:

$$-U_K = \frac{1}{2} m v_2^2 - \frac{Z_2 e^2}{r} \tag{2.15}$$

The integral over v_2 may be transformed to:[16,26]

$$\int f(v_2)\,dv_2\,\frac{d\sigma}{d\Delta E}(\Delta E, v_1, v_2) = \int d^3\vec{r}\,\rho(r)\,\frac{d\sigma}{d\Delta E}(\Delta E, v_1, v_2(r))$$

$$= \int 2\pi b\,db \int_{-\infty}^{\infty} dz\,\frac{d\sigma}{d\Delta E}(\Delta E, v_1, v_2([b^2+z^2]^{1/2}))\,\rho([b^2+z^2]^{1/2}) \tag{2.16}$$

where $\rho(r)$ is the electronic density. The probability, P(b,E), can be defined as

$$P(b,E) = \int_{u_K}^{\infty} d\Delta E \int_{-\infty}^{\infty} dz\,\frac{d\sigma}{d\Delta E}(\Delta E, v_1, v_2([b^2+z^2]^{1/2}))\,\rho([b^2+z^2]^{1/2}) \tag{2.17}$$

P(b,E) scales similar to Eq. (2.8) and tabulations of scalable probabilities are available.[16]

The cross section obtained in this way generally agrees very well with experiment and with the PWBA and SCA theories.[1] Few measurements have been made of impact parameter probabilities. In this case the SCA theory gives different predictions for P(b,E), but so far, it is not possible to say which theory gives better results.[27]

A common criticism of the BEA theory is that it does not take into account the distortion of the target K shell wavefunction and, therefore, of $f(v_2)$ due to the presence of the projectile. For very heavy projectiles this distortion results in increased binding of the K electron, because it is attracted to both the projectile and target nuclei. The added binding shifts $f(v_2)$ to higher average velocities. This criticism however is not limited to the BEA theory but to the SCA and PWBA theories as well. All assume that the initial and final atomic wavefunctions are not affected by the projectile atomic number, i.e.

Z_1 is sufficiently small compared to Z_2, so that very little distortion and increased binding takes place. Attempts have been made within the framework of the BEA theory to take into account the added binding effect by using the UA charge $Z_1 + Z_2 - 0.3$ in place of $Z_2 - 0.3$ and the UA binding energy instead of the SA binding energy where ever these quantities appear.[57] This has met with some success in predicting total cross sections and has recently been partially justified theoretically by Basbas *et al*,[73] Madison and Merzbacher,[13] and Briggs.[28] Still, the PWBA, SCA, and BEA theories are basically unusable if one wishes to calculate cross sections and impact parameter probabilities in heavy ion collisions where these distortion and binding effects become overwhelmingly important.

2.4 The Method of Perturbed Stationary States (PSS)[18,19]

The PSS method accounts for the added binding effect by recognizing that the wavefunctions and energy levels should be eigenfunctions of the molecular Hamiltonian:

$$H = -\frac{\hbar^2 \nabla^2}{2m} - \frac{Z_1 e^2}{|\vec{R}_1(t) - \vec{r}|} - \frac{Z_2 e^2}{|\vec{R}_2(t) - \vec{r}|} \tag{2.18}$$

where $\vec{R}_1$ and $\vec{R}_2$ are the nuclear coordinates of the projectile and the target nucleus. Both the energy levels and wavefunctions are functions of time through their dependence on the internuclear distance R. As in the SCA theory, the amplitude for excitation is calculated:

$$a(\varepsilon_f, b, E, \infty) = \int_{-\infty}^{\infty} dt \langle \psi_f(t) | V(t) | \psi_i(t) \rangle \times \exp\left[i \int_{-\infty}^{t} (\omega_f(t') - \omega_i(t')) dt' \right] \tag{2.19}$$

There the perturbing potential is:

$$V(t) = \hbar \frac{d}{dt} = \hbar\left(\dot{R}\frac{\partial}{\partial R} + \dot{\theta}\frac{\partial}{\partial \theta}\right) \tag{2.20}$$

where θ is the angle between the beam direction and the internuclear axis. Coupling due the first term is called radial coupling. States of the same parity and angular momentum projection Λ along the internuclear axis are coupled together. The second perturbation causes Coriolis or Rotational coupling and states of the same parity but Λ quantum numbers differing by ±1 are coupled together. If the collision takes place in the X-Z plane with the incident projectile moving parallel to the Z axis, the term $\dot{\theta}\frac{\partial}{\partial\theta}$ may be written in the UA limit as:

$$\dot{\theta}\frac{\partial}{\partial \theta} \approx \frac{bv}{R^2}\frac{1}{\sqrt{2}}\left(L_+ \pm L_-\right) \tag{2.21}$$

where L_+ and L_- are the familiar raising and lowering operators.

Implicit in the PSS method is the requirement that the projectile should be moving sufficiently slow to justify the use of adiabatic molecular wavefunctions as a basis set. For the $1s\sigma$ wavefunction, "sufficiently slow" means $v_1/v_K \ll 1$ or at least $v_1/v_K \lesssim 1$. Clearly if the K electron velocity v_K is much greater than the projectile velocity v_1, the electron is moving fast enough to adjust its motion to the presence of the projectile's Coulomb field. If it is moving much slower than the projectile, however, we can imagine that the projectile completely traverses the K shell before the K electron wavefunction distorts very much from its atomic wavefunction. For excited states the same criterion applies except that v_K is replaced

by v_c, the electron velocity appropriate to the state in question. This implies that there is always a band of states below and in the continuum which cannot be described adiabatically. Thorson[19,32] defines the limits of this band for $H^+ + H$ collisions, but those limits are general:

$$\epsilon_c \approx \frac{1}{4}\frac{E_1 m}{A_1 M} \tag{2.22}$$

where E_1 is the (lab) ion energy and A_1M is the mass of the projectile ion. This is equivalent to $v_1/v_c < 2$, and the difference between this criterion and $v_1/v_c < 1$ is insignificant. Much effort has been devoted to obtaining outer shell adiabatic 3sσ, 4sσ, 4pσ, 4sσ, etc. molecular wavefunctions for systems as light as Ne + Ne.[33] Clearly, though, these wavefunctions are virtually useless in collision problems if they do not meet the preceding criterion.

In Fig. 2, the energy levels of states described by MOs are drawn as a function of the internuclear distance. Aside from the two kinds of coupling that were discussed, transitions between MOs may be usefully classified as degeneracy mediated processes or processes requiring energy transfer.

Some typical examples of degeneracy mediated processes can be seen in these diagrams. For instance at the crossing of the 3dσ and 3sσ energy levels, Landau-Zener transitions due to radial coupling may occur.[29] An electron initially in the 3dσ orbital has a probability of jumping to the 3sσ orbital as the two nuclei come together and a probability 1-w of staying in the 3sσ orbital on the outgoing part of the collision. Neglecting quantum mechanical interference effects,

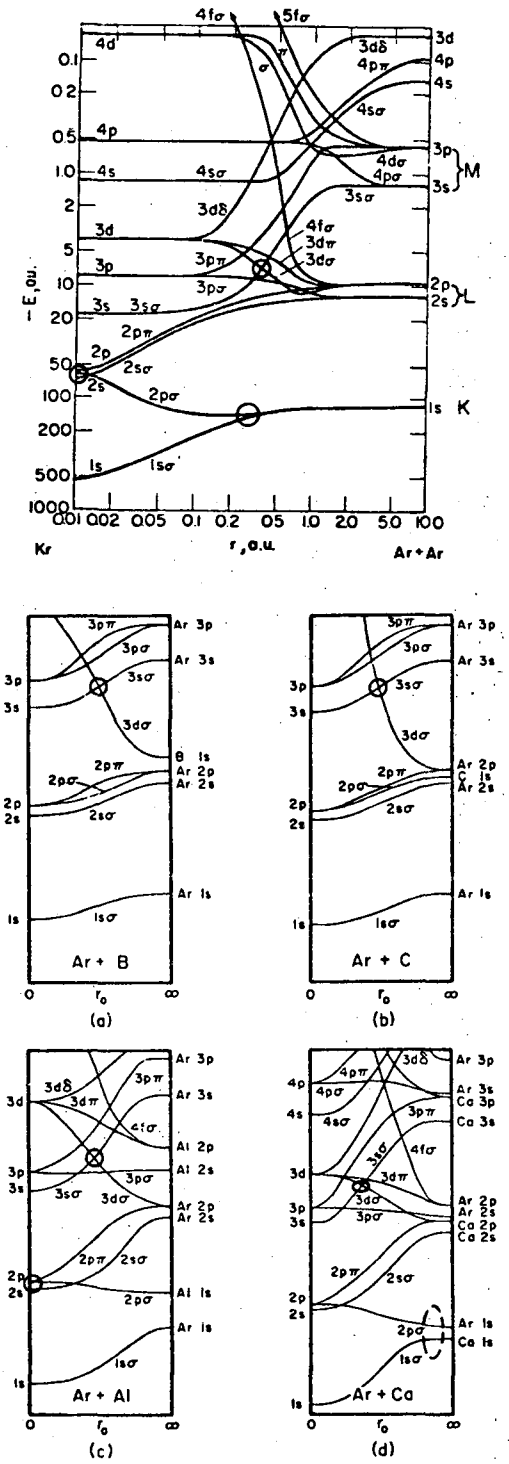

XBL 7511-8988

Fig. 2. Molecular level diagrams for symmetric and various asymmetric collisions involving Ar atoms (from Garcia *et al*[1]). Vertical scale is binding energy, horizontal scale represents internuclear distance. Transition regions of interest are circled (see text).

the total probability for an electron jumping from the 3dσ orbital to the 3sσ orbital in a complete collision is 2w(1-w). Another degeneracy mediated process can occur at small internuclear distances where the 2pσ and 2pπ orbitals overlap. Coriolis coupling mixes the two wavefunctions so that a 2pσ electron may jump to the 2pπ orbital in the collision.[9] Still another example can occur at large internuclear distances where the 2pσ and 1sσ orbitals approach each other. There radial coupling can mix the 1sσ and 2pσ MOs strongly. A 1sσ electron may be promoted into the 2pσ orbital if there is a vacancy in that orbital. This process is called Demkov coupling[30] or vacancy sharing.[31]

Degeneracy mediated processes are classed as such because they usually involve an electron jump from one MO to another at an internuclear distance where the MO energy levels are degenerate. The energy levels need not be exactly degenerate; it is sufficient that the energy difference be small.* In this regard, the Demkov process is not exactly a degeneracy mediated process when applied to asymmetric collisions where the 2pσ - 1sσ energy difference is finite at large R. It is a degeneracy mediated process for $Z_1 \cong Z_2$ and a process requiring energy transfer for Z_1 much different than Z_2.

Processes requiring energy transfer are comparatively weak. The proton ionization of a K electron in a heavy target atom is such a process. Likewise, in a near symmetric collision, the excitation of an electron from the 1sσ, 2pσ, and other tightly bound molecular

---

*I have no definition of sufficiently "small". Probably, the energy transfer ΔE should be smaller than the equivalent-electron projectile energy $mE_1/(A_1M)$.

orbitals to the continuum is also a process requiring a large energy transfer. The $1s\sigma$ electron can also be excited to the $2p\pi$ orbital and other less tightly bound MOs, and this process would also require a large energy transfer. As opposed to degeneracy mediated processes, processes requiring energy transfer involve an electron jump from one MO to another MO which are separated in energy at all internuclear distances by a finite amount.

The classification of electronic excitation processes into these two different kinds of processes is a classification into strong and weak processes. When energy transfer is required, the probability of exciting electrons in the molecule is small. This can be seen by examining the oscillatory part of the integral in Eq. (2.19). Let us take $\int_0^t (\omega_f(t') - \omega_i(t'))dt'$ as approximately ωt, and for excitation out of the $1s\sigma$ orbital $\hbar\omega$ is of the order of U_K. We expect that the matrix element, $V_{fi}(t)$ in Eq. (2.19) peaks or falls off over a distance $R = a_K$. Hence over the range of the integration ($\sim 4a_K$) the integrand undergoes $v_K/(\pi v_1)$ oscillations. Since $v_1/v_K << 1$ in order for the molecular model to hold, there will be many oscillations similar to what is shown in Fig. 3. A small final amplitude will result when we integrate $\dot{a}(t)$. In the real part of $\dot{a}(t)$, positive contributions coming from positive values of the $\cos\left(\int_0^t (\omega_f(t') - \omega_i(t'))dt'\right)$ are cancelled out by negative contributions coming from negative values of the cosine. Note that in the $1s\sigma$ orbital $\hbar\omega(R)$ becomes much greater than U_K at small R. This will simply mean that the integrand oscillates more rapidly over the range of integration. The $2p\sigma$ energy gap stays approximately constant in symmetrical collisions and equal to U_K.

$$\mathrm{Re}[\dot{a}(i\varepsilon,b,E,t)] = V(t)\cos\int_{-\infty}^{t}\Delta\omega(t')dt'$$

ENERGY TRANSFER

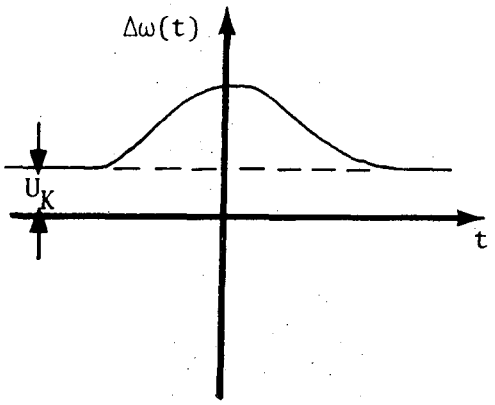

$$\int\Delta\omega dt' \approx \frac{U_K R}{\hbar v_1} = \frac{v_K}{2v_1}\,\frac{R}{a_K}$$

DEGENERACY MEDIATED

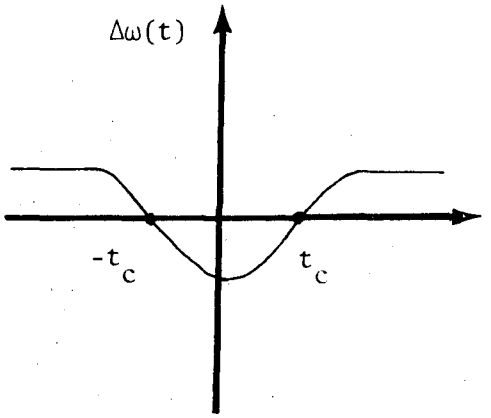

$$\Delta\omega(t_c) = 0$$

$$\frac{v_1}{v_K} << 1 \rightarrow \int\Delta\omega dt' >> 1$$

$$\int_{t_c-\Delta t}^{t_c+\Delta t}\Delta\omega dt' << 1$$

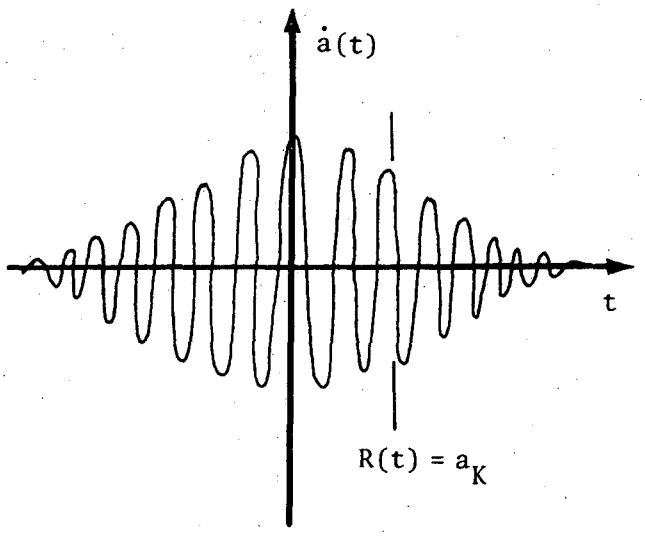

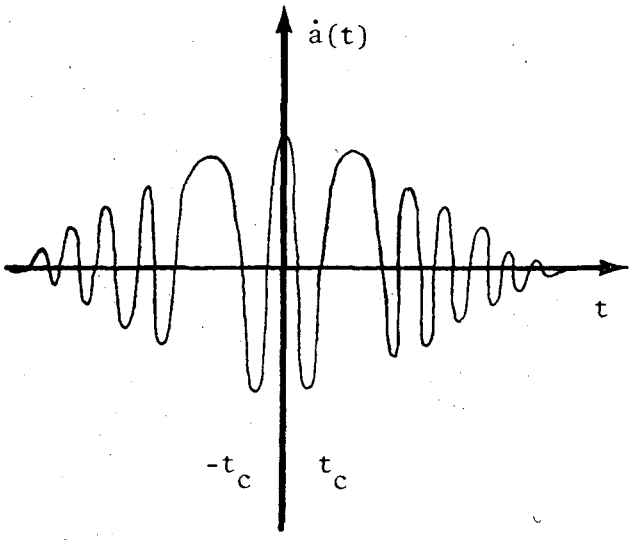

$$a(i\varepsilon,b,E,\infty) = \int_{-\infty}^{\infty} dt V(t)\, e^{i\int_{-\infty}^{t}\Delta\omega(t')dt'}$$

a(∞) small

a(∞) large

FIGURE 3

In degeneracy mediated processes, however, there is an internuclear distance or time where $\omega_f(t) = \omega_i(t)$. At this point the integrand in Eq. (2.19)† temporarily stops oscillating. In integrating from $-\infty$ to $+\infty$, there will be two large, positive contributions to the real or imaginary parts of the amplitude (depending on whether $V_{fi}(t)$ is even or odd in time). The resulting probability for the excitation of an electron can be very large.

This argument emphasizes the importance of the energy gap in its effect on the amplitude for the excitation of electrons from MOs. The energy gap is much more important than the matrix elements. In calculating a probability for some process requiring energy transfer, if we were to decrease the magnitude of the matrix elements by a factor of two, or if we increased the energy gap by a factor of two, both effects would decrease the probability. The change due to affecting the energy gap, however, would be very much larger. Finally all that we have said here is true only where $v_1/v_K \ll 1$, i.e., where the molecular model applies. The importance of the energy gap will be less and the classification into degeneracy mediated and energy transfer processes will break down when v_1/v_K approaches unity. Clearly, if $v_1/v_K \gg 1$, then the integrand in Eq. (2.19) will not oscillate at all, and it will be the matrix elements that will determine the electron excitation probabilities.

A modification that must be made to the wavefunctions in the PSS method is to include translation factors. The point of origin of

---

†Equation (2.19) can only strictly be used for weak coupling processes. For strong processes, one has to solve coupled differential equations [see Eq. (B.4)].

the molecular wavefunctions is the center of mass of the colliding system and not the moving projectile or recoiling target atom. To preserve Galilean invariance the molecular wavefunctions are modified to include a factor:[19,34,35]

$$\psi_{MO}(\vec{r},\vec{R}) \rightarrow \psi_{c.o.m.}(\vec{r},\vec{R})\exp[im\vec{v}\cdot\vec{R}\, f(\vec{r},\vec{R})/\hbar + imv^2 t/2\hbar] \tag{2.23}$$

where v is the velocity of the center of mass in the lab system and $f(\vec{r},\vec{R})$ is a function which must have the following properties:

$$f \rightarrow +1 \quad \text{when} \quad |\vec{R}_1(t) - \vec{r}| \gg |\vec{R}_2(t) - \vec{r}|$$

$$f \rightarrow -1 \quad \text{when} \quad |\vec{R}_1(t) - \vec{r}| \ll |\vec{R}_2(t) - \vec{r}|$$

$$f \rightarrow 0 \quad \text{when} \quad R \rightarrow 0 \tag{2.24}$$

and f must preserve orthogonality between wavefunctions. The importance of the translation factor increases with the amount of energy transferred.[36] In degeneracy mediated processes, it can be neglected. The main effect of the factor is to modify the matrix elements; without it, some matrix elements tend to be spuriously large at large internuclear distances. A suitable choice of $f(\vec{r},\vec{R})$ minimizes these spurious contributions. Together with the difficulty of evaluating the highly oscillatory trajectory integrals, the difficulties of optimizing the translation factors to preserve the conditions of Eq. (2.24) and of reducing spuriously large matrix elements make the PSS method a difficult method to use.

For symmetric collisions, the impact parameter probability and cross sections calculated with the method of PSS obey the following

scaling relations:[37]

$$P^{Z}(b/a_K, \eta_K^{Z}) = P'(b/a_0, \eta_K^{H})$$
$$\sigma^{Z}(\eta_K^{Z}) = \frac{1}{Z^2}\sigma'(\eta_K^{H}) \tag{2.25}$$

where $Z_1 = Z_2 = Z$, a_0 is the Bohr radius, and η_K^H and η_K^Z are the familiar scaling parameters defined for the PWBA scaling law [Eq. (2.3)] for p + H collisions and Z + Z collisions respectively. This scaling law ignores the effects of Coulomb repulsion and screening. For symmetric collisions, the distance of closest approach of the two nuclei in head-on collisions is

$$d_0 = \frac{2Z^2e^2}{E_1} \approx \frac{0.00218}{\eta_K}\frac{Z}{A_1}a_K \tag{2.26}$$

The scaling relations will only hold if Z/A_1 is kept constant. Since in medium-Z heavy ion collisions $Z/A_1 \approx \frac{1}{2}$, it is better to use $D^+ + D$ cross sections instead of $H^+ + H$ cross sections in Eq. (2.25). It is also easy to calculate cross sections for hypothetical particles of charge 1 and mass A/Z. We expect that Coulomb repulsion effects will be small; therefore this will change the results in only a minor way.

For asymmetric collisions, the following relations must hold if we neglect Coulomb repulsion effects:[38]

$$P^{Z_1}(Q, b/a_{K_1}, \eta_K^{Z_1}) = P'(Q, b/a_0, \eta_K^{H})$$
$$\sigma^{Z_1}(Q, \eta_K^{Z_1}) = \frac{1}{Z_1^2}\sigma(Q, \eta_K^{H}) \tag{2.27}$$

where Q is the ratio of Z_2 to Z_1. We should mention that the solution of two-center one-electron wavefunctions is not limited to integral atomic numbers. Therefore, Br + Zr cross sections could easily be found by scaling p + (Z = 1.1428) cross sections.

One of the important open questions in K vacancy production is the dependence of P^Z and σ^Z on Q. So far this question has been examined only for the $2p\sigma - 2p\pi$ promotion process.[38] In other cases an experimental approach has been attempted, as described below.

We have made a PSS calculation for excitation of a $1s\sigma$ electron to the continuum and return to this method in a later chapter.

III. EXPERIMENT

Although from the point of view of the PSS theory, K vacancies are made in MOs, one usually measures the K x rays of the separated atoms. Extensive measurements of K x ray cross sections for heavy ion bombardments with a wide variety of targets had not been made previously except for a couple of cases. Kubo *et al*[39] made a series of cross section measurements with 45 to 94 MeV Ni ions and 45 to 110 MeV Br ions. Meyerhof *et al*[10] made thick target yield measurements with 30 and 60 MeV Br and 47 and 80 MeV I ions. In this chapter we report on measurements made with 200 MeV Kr ions at the Berkeley SuperHILAC.

When we began this work, the theory of K vacancy formation was not developed to the point (and still isn't) where highly precise cross sections were required. We thought it more useful to make survey experiments with a wide range of targets and to measure thick target yields rather than concentrating on single systems obtaining, for instance, the ion energy dependence of cross sections using gas targets or very thin foils. Theoretical thick target yields may be obtained from predicted cross sections fairly accurately, and cross sections may be obtained from experimental thick target yields less accurately. Except for the multi-collision mechanism which affects the experimental $2p\sigma$ cross sections, as will be described below, no other solid state effects that we know of affect our extracted cross sections sufficiently to change the conclusions we draw from them. In particular, for the high energy heavy systems of interest here, recoil effects are not important.[74] Since our interest was to examine the regions where strong and weak coupling mechanisms prevail, we had to do measurements of yields differing by six orders of magnitude or more. Therefore, cross sections

accurate to within a factor of two seemed a sufficient goal. This chapter describes the measurement of thick target yields and the following chapter describes the results.

Figure 4 shows a schematic of the experimental setup. A 200 MeV $^{84}Kr^{+21}$ beam entered the target chamber through a 0.125 to 0.1875 inch collimator and was directed onto a thick (0.0005 to 0.005 inch) foil tilted 45° or 60° to the beam direction. The entire chamber was insulated from the beam line and the beam current was monitored by connecting the chamber to an integrator (made by Brookhaven Instruments Corporation). An electron suppressor was sometimes used between the collimator and chamber to prevent both a spray of electrons scattered from the collimator from entering the chamber and a back-spray of electrons from the target from leaving the chamber. An intrinsic Ge x ray detector with 0.010 inch beryllium window viewed the front of the target through an 0.001 inch beryllium window on the chamber. An intrinsic Ge planar or Ge(Li) coax γ-ray detector viewed the back of the target. Its main purpose was to provide an instantaneous relative measure of the beam intensity to feed into the deadtime circuit (see below). Depending on the x ray energy and its intensity, the x ray detector-to-target distance was varied from 1.25 to 7 inches. Calibrated Al absorbers were sometimes used to attenuate unwanted radiation. Photons between 4 and 200 keV were detected in this work.

To measure the deadtime of the counting system we used a "crossed detector trigger system". Signals from the fast discriminator on the γ-ray detector were fed into a pre-scalar that provided one pulse for every 10 to 10,000 input pulses. The scale down factor was varied depending on the counting rate. This pulse was delayed 150

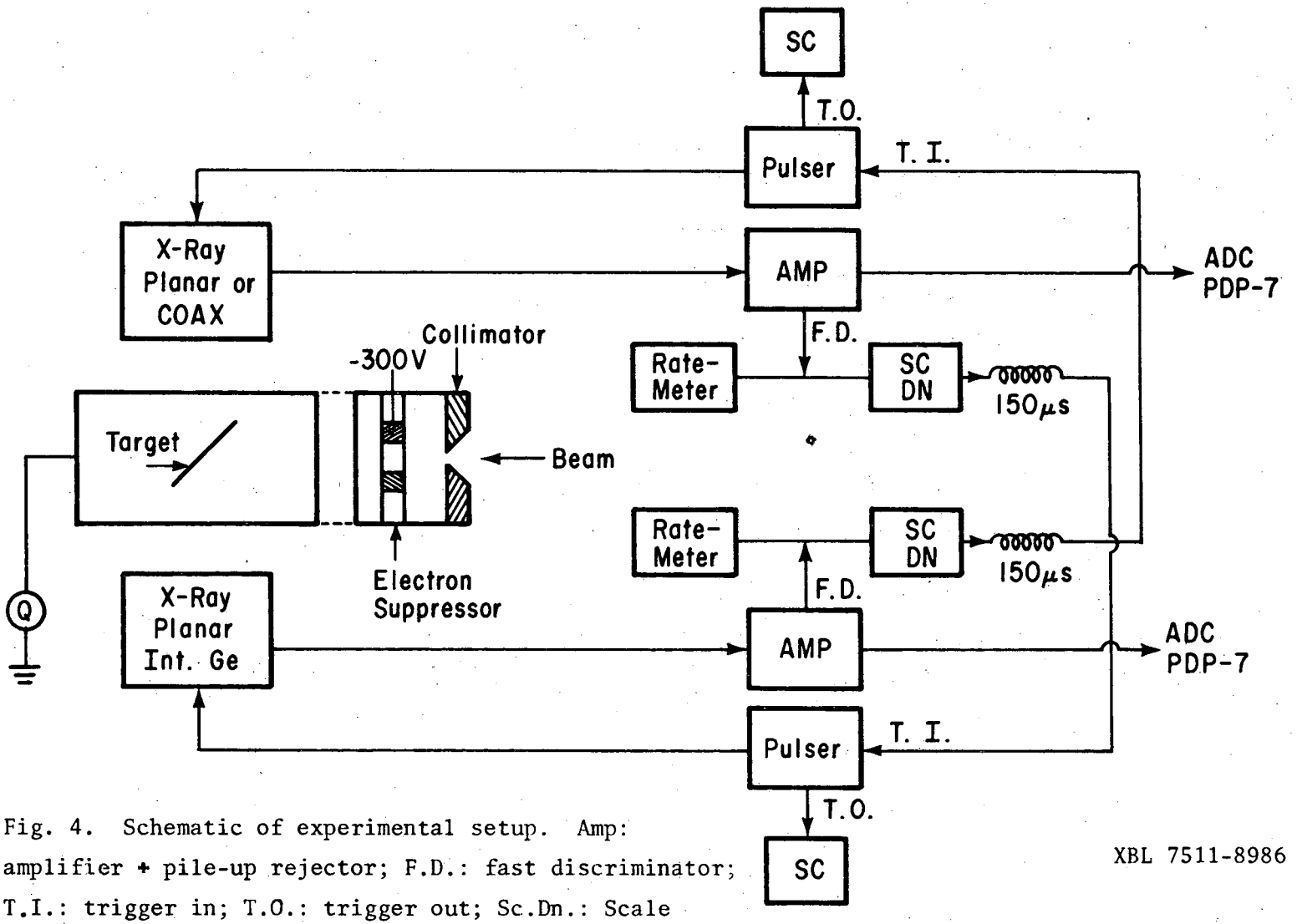

Fig. 4. Schematic of experimental setup. Amp: amplifier + pile-up rejector; F.D.: fast discriminator; T.I.: trigger in; T.O.: trigger out; Sc.Dn.: Scale down; S.C.: Scaler; Q: integrator.

XBL 7511-8986

μsec which then triggered the pulser on the x ray detector. The number of pulses fed into the x ray detector was recorded and the number of pulses appearing in the discrete pulser peak in the x ray spectrum was later determined. The deadtime correction D is the ratio of these two quantities; it generally varied between 1.00 and 1.5.

A pulsed opto pre-amplifier was used for the x ray detector[40] and a standard resistor feedback pre-amplifier was used for the γ-ray detector. Pileup rejectors, having better than 200 nsec pulse pair resolution, were always employed. Data was taken on Diamond and Stephens' PDP-7 computer system[41] and peak summing, background subtraction, and other data analysis was also done on that system.

The yield of x rays of energy E_x in photons per projectile is defined as:

$$Y(E_x) = \frac{CDqA}{QFG \cdot 6.25 \times 10^{18}} \tag{3.1}$$

where C is the number of counts in the x ray peak of energy E_x, Q is the number of coulombs of charge as measured by the beam integrator, q is the charge state of Kr $+21 \pm 2$, A is the attenuation corrections for absorption by air, by the beryllium window, and by any aluminum absorbers placed between the detector and the chamber,[42,43] $F(E_x)$ is the efficiency of the x ray detector taken at a standard distance using calibrated γ-ray sources, and G is the geometry factor which corrects F to the actual distance from the target to the detector. The geometry factor is not expected to be photon energy dependent for this thin planar detector.

The uncertainties in these quantities were estimated to be:

Q,q	-	10%
F,G	-	15%
A	-	15%
D	-	5%
C	-	1 to 100%

Generally the yields were very high and many counts could be obtained so the statistical uncertainty in C is small. For the K x rays of targets with $Z > 80$, however, few counts were obtained with a consequent increase in the statistical uncertainty. Most serious are cases where the K lines of the projectile lie in the region of the L or K lines of the target atom (Kr + Au, Pb, Bi, and U and Kr + Br, Y). In these cases high uncertainties resulted.

Assuming the Kα and Kβ peaks are clearly separated ($Z \gtrsim 25$), the yield of K vacancies is

$$Y = [Y(K\alpha) + Y(K\beta)] / \omega_K \tag{3.2}$$

where ω_K is the fluorescent yield.[44] Since most fluorescent yields in this work were on the order of unity, any change in ω_K due to high stripping of the target or projectile should be small. Fluorescent yields do not change appreciably from their neutral atom values unless the atom is stripped to much less than ten electrons, an unlikely possibility at these low energies. Hence neutral atom values of ω_K were used in this work.[44]

If theoretical cross sections were available, they could be compared with thick target yields by integrating over the range of ion energy. Assuming the target is tilted 45° to the beam and the detector views the front face of the target at right angles to the beam, the yield is[14]

$$Y_x(E_1) = n_2 \int_0^{E_1} dE\, \sigma_x(E)\, S(E)^{-1} e^{-\mu R(E)} \tag{3.3}$$

where n_2 is the target atom density, S(E) is the stopping power of a Kr ion of energy E in the target material,[45] R(E) is the thickness that an ion initially of energy E_1 has penetrated before slowing down to energy E, and μ is the attenuation coefficient for the Kα or Kβ x-ray of Kr or the target atom in the target material.[42,43] Since the maximum penetration of the ion is only about 0.001 cm, the absorption factor can be neglected except for very low energy x-rays. Expression (3.3) is not valid if recoil effects are important, but we have verified that they are not for the cases of interest.

Differentiating Eq. (3.3) one can obtain the cross section if the energy dependence of the yield is known:

$$\sigma(E_1) = \frac{1}{n_2} \frac{dY}{dE}\bigg|_{E_1} S(E_1) + \frac{\mu}{n_2} Y(E_1) \tag{3.4}$$

To obtain approximate cross sections, we have fitted the yield to a simple power law:

$$Y(E) \sim E_1^{\,m}$$

then

$$\sigma(E_1) = \frac{m}{n_2} \frac{Y(E_1)}{E_1} S(E_1) + \frac{\mu}{n_2} Y(E_1) \tag{3.5}$$

By comparing 30 and 60 MeV Br (Z = 35) yields with 200 MeV Kr (Z = 36) yields and 47 MeV I (Z = 53) yields with 325 MeV Xe (Z = 54) yields, we have obtained m values accurate to about 20% for each projectile and target yield. Cross sections accurate to about ±40% could therefore

be obtained.

For encounters between Kr ions and target atoms with $60 < Z < 92$, the target K yields are complicated by background due to nuclear events. With the exception of Pb and Bi, nuclei found in nature in this region tend to be deformed and have low lying states which are strongly Coulomb excited by 200 MeV Kr ions.[51] This excitation is followed by the emission of a γ-ray or internal conversion. In internal conversion, the transition energy is used to eject an inner shell target electron into the continuum, thereby making inner shell vacancies. A conversion coefficient $\alpha_K(Z_2,\lambda\pi,E_\gamma)$ which gives the number of K vacancies created per γ-ray emitted can be computed.[52] It depends on the target atomic number and the multi-polarity, parity, and energy of the γ-ray transition. If the number of γ-rays from each excited state is measured, the total number of K vacancies formed is:

$$Y_K = \sum_i \alpha_{Ki}\, Y(E_{\gamma i}) \tag{3.6}$$

The yield of γ-rays can be obtained similar to the way the yield of $K\alpha$ or $K\beta$ x-rays was obtained. A Kr ion impinging on a nucleus in this region may easily excite the first five or six nuclear states in the ground rotational band. In principle, therefore, all we need to do is measure the γ-ray yields and use theoretical conversion coefficients (reliable to within 2%) to obtain the background K vacancy yield. This can be subtracted to obtain the atomic excitation yield. The subtraction of two numbers which have relative errors of 10% or more introduces serious uncertainty. We discuss the data in detail in Appendix A.

Most of our work was done at 200 MeV, an energy which is effectively as low as a SuperHILAC beam can be well focused, but which is not so high as to destroy adiabacity ($v_1/v_K \sim 0.3$). Also at higher energies ($\gtrsim$ 330 MeV), the Kr ion has enough energy to exceed the Coulomb barrier in many light nuclei. Hence nuclear reactions occur which complicate the interpretation of the SA yield.

IV. EXPERIMENTAL RESULTS

Aside from the experimental problems of relating thick target yields of SA x-rays to cross sections, there is the theoretical problem of relating the cross sections for SA x-rays to cross sections for excitation out of molecular orbitals. A vacancy in the heavier or lighter collision partner could have been formed in a number of different ways in the quasi-molecule during the collision. Therefore, the interpretation of the data is not straightforward.

4.1 Basic Relations

During a collision, a vacancy may be formed in either the $2p\sigma$ MO or the $1s\sigma$ MO. How it is formed in each MO is discussed below. Here we point out that although the $2p\sigma$ MO correlates to the K shell of the lighter collision partner, and the $1s\sigma$ to the heavier collision partner on our correlation diagrams, this does not mean that $2p\sigma$ vacancies necessarily end up in the K shell of the lighter and $1s\sigma$ vacancies necessarily end up in the K shell of the heavier partner. The $2p\sigma$ and $1s\sigma$ orbitals are strongly Demkov coupled at large distances.[30,31] We can define a probability w that during the outgoing part of the collision, a vacancy in the $2p\sigma$ orbital jumps to the K shell of the higher-Z partner, or conversely, a $1s\sigma$ vacancy jumps to the lower-Z partner. Then the cross section for making vacancies in the heavier (H) and lighter (L) partner is:

$$\sigma_K(L) = (1-w)\,\sigma_{2p\sigma} + w\,\sigma_{1s\sigma}$$
$$\sigma_K(H) = (1-w)\,\sigma_{1s\sigma} + w\,\sigma_{2p\sigma} \qquad (4.1)$$

The 2pσ cross section is much larger than the 1sσ cross section so:

$$\sigma_K(L) \approx (1-w)\,\sigma_{2p\sigma} \tag{4.2a}$$

$$\sigma_K(H) = (1-w)\,\sigma_{1s\sigma} + w\,\sigma_{2p\sigma} \tag{b}$$

and within the same approximation,

$$\sigma_{2p\sigma} = \sigma_K(H) + \sigma_K(L) \tag{c}$$

$$\sigma_{1s\sigma} = \frac{1-w}{1-2w}\,\sigma_K(H) - \frac{w}{1-2w}\,\sigma_K(L) \tag{d}$$

In the limit where the energy difference between the 2pσ and 1sσ orbitals approaches zero (symmetric collisions):

$$\sigma_K(L) \rightarrow \sigma_K(H) \rightarrow \frac{1}{2}\,\sigma_{2p\sigma} \tag{4.3}$$

Because of the large difference between the 2pσ and 1sσ cross sections, it is impossible to extract the 1sσ cross section in symmetric or near symmetric collisions by measuring the x-rays of the higher-Z SA. It is necessary for w to be small so that the second term in Eq. (4.2d) can be neglected

A simple formula for the probability w was developed by Demkov[30] and Meyerhof[31] for collisions with zero impact parameter. Assuming $\sigma_{1s\sigma}$ can be neglected, the formula predicts that the ratio of vacancies in the higher to the lower collision partner should be:

$$\frac{\sigma_K(H)}{\sigma_K(L)} = \frac{w}{1-w} = e^{-2x} \tag{4.4}$$

where

$$\begin{aligned} 2x &= \pi\hbar\,/\,U_K^{\frac{1}{2}}(H) - U_K^{\frac{1}{2}}(L)\,/\,/(2m)^{1/2}\,v_1 \\ &= \frac{2\pi}{v}\,/\,I^{1/2}(H) - I^{1/2}(L)\,/ \end{aligned} \tag{4.5}$$

Here, v is the ion velocity in atomic units (2.18×10^8 cm/sec) and I(H) and I(L) are binding energies in keV. This formula was first applied by Meyerhof[31] to a great amount of Ni, Br, and I data and was found to fit particularly well. Since then other experimental work confirmed the formula.[46] Also PSS calculations have given results in accord with the simple formula.‡[47,48]

The cross section for the production of vacancies in the 2pσ and 1sσ orbitals comes from contributions from the following terms:

$$\sigma_{2p\sigma} = \sigma_R + \sigma_C^u + \sigma_{HS}^u + \sigma_{M.S.} + \sigma_{M.C.}$$

$$\sigma_{1s\sigma} = \sigma_C^g + \sigma_{HS}^g \tag{4.6}$$

Here σ_R is the cross section for the 2pσ to 2pπ rotational coupling transition,[59] σ_C is the ionization cross section,[19] σ_{HS} is the cross section for excitation to high lying bound states excluding the 2pπ orbital, and σ_{MS} is the multi-step cross section where an initial M or N shell vacancy Demkov couples into the 2pπ orbital early in the collision allowing 2pσ - 2pπ transitions to take place.[49,50] If the projectile is the higher-Z collision partner, a multi-collision process can occur in which a projectile L vacancy lives long enough to enter the 2pπ orbital in a second collision, again allowing 2pσ - 2pπ transitions to occur. The corresponding cross

---

‡Deviations have been noted: Taulberg *et al*[75] have done PSS calculations that predict deviations at high velocities in asymmetric collisions. Taulberg and Briggs[47] also predicted deviations at very low velocities in Ne + O collisions, but recently reported that those deviations were due to numerical errors in their computer code. Stolterfoht *et al*[46] have experimentally observed deviations in very light collision systems ($Z < 6$).

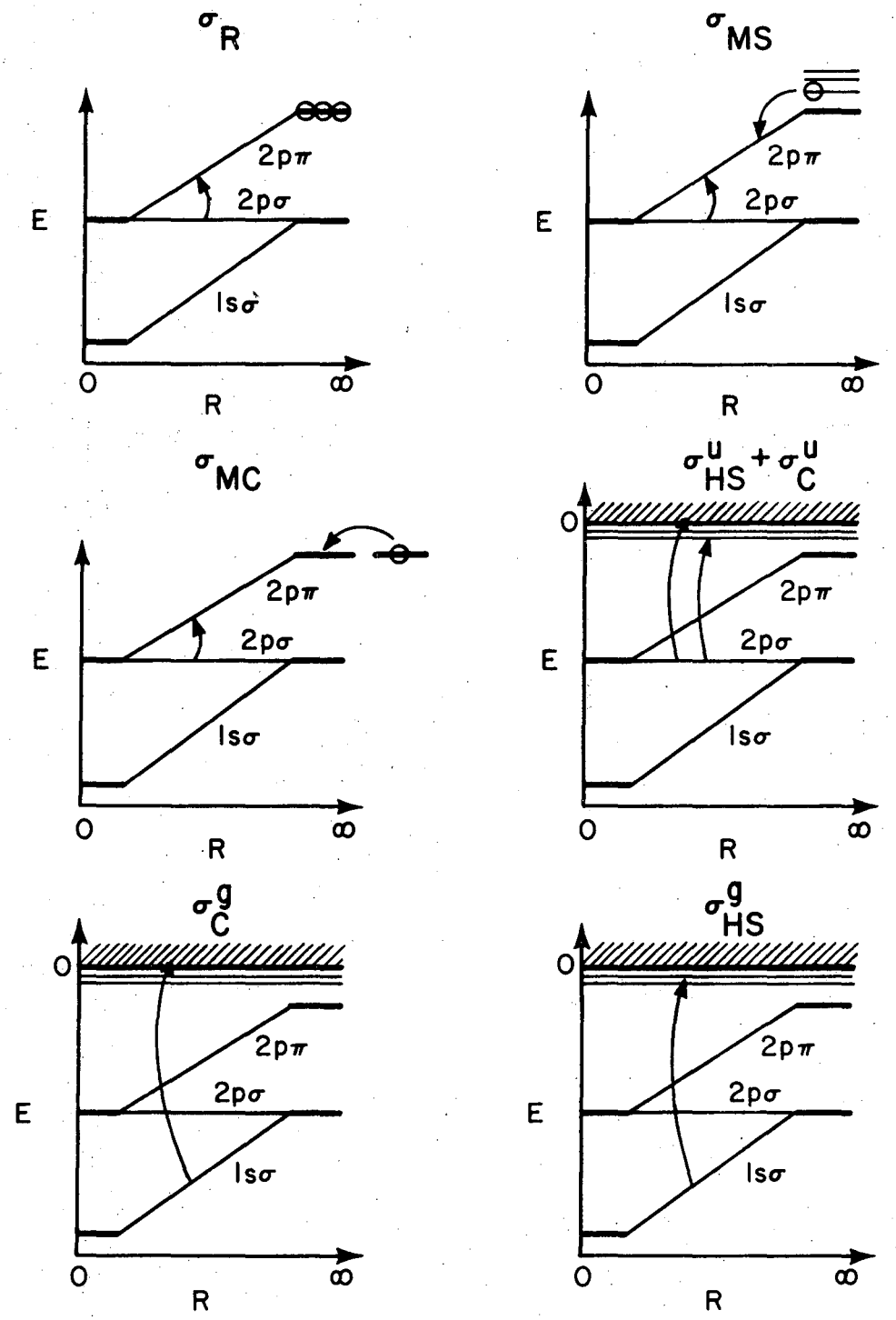

XBL 7511-8990

Fig. 5. Correlation diagrams for arbitrary symmetric encounters showing possible excitation processes.

section is called σ_{MC}. One other possibility is a multi-collision-multi-step process. If the projectile is the lighter partner, projectile L vacancies may live long enough to enter a second collision and Demkov couple into the $2p\pi$ orbital early in the second collision. We shall consider such a process as a multi-collision process.

If the rotational coupling process were not so strong the multi-collision and multi-step processes would not be important. Normally rotational coupling is blocked in the systems of interest to us because no initial $2p\pi$ vacancies are present in projectile and target atoms with $Z > 10$. Even Kr^{+21} has all of its L shell filled so that no rotational transitions are allowed using this highly stripped projectile. Effectively, the multi-collision and multi-step processes allow $2p\sigma$ - $2p\pi$ rotational coupling to take place even in systems where $Z > 10$ by providing vacancies in the $2p\pi$ orbital by means other than stripping the collision partners down to less than ten electrons. No process analogous to the strong rotational coupling process takes place in the $1s\sigma$ orbital so multi-collision and multi-step terms need not be included there.

Finally, Eqs. (4.1) to (4.6) apply only where $Z_1/2 < Z_2 < 2Z_1$. Outside of this region, the projectile or target K shell will correlate to shells other than the $2p\sigma$ and $1s\sigma$, hence the SA yields may be a measure of $3d\sigma$ excitation or some other process.

4.2 Thick Target Yield Data

Figure 6 shows projectile and target thick target yields for 200 MeV $^{84}Kr^{+21}$ ions. This figure was originally prepared to compare the cross section for these nearly symmetric collisions with PWBA

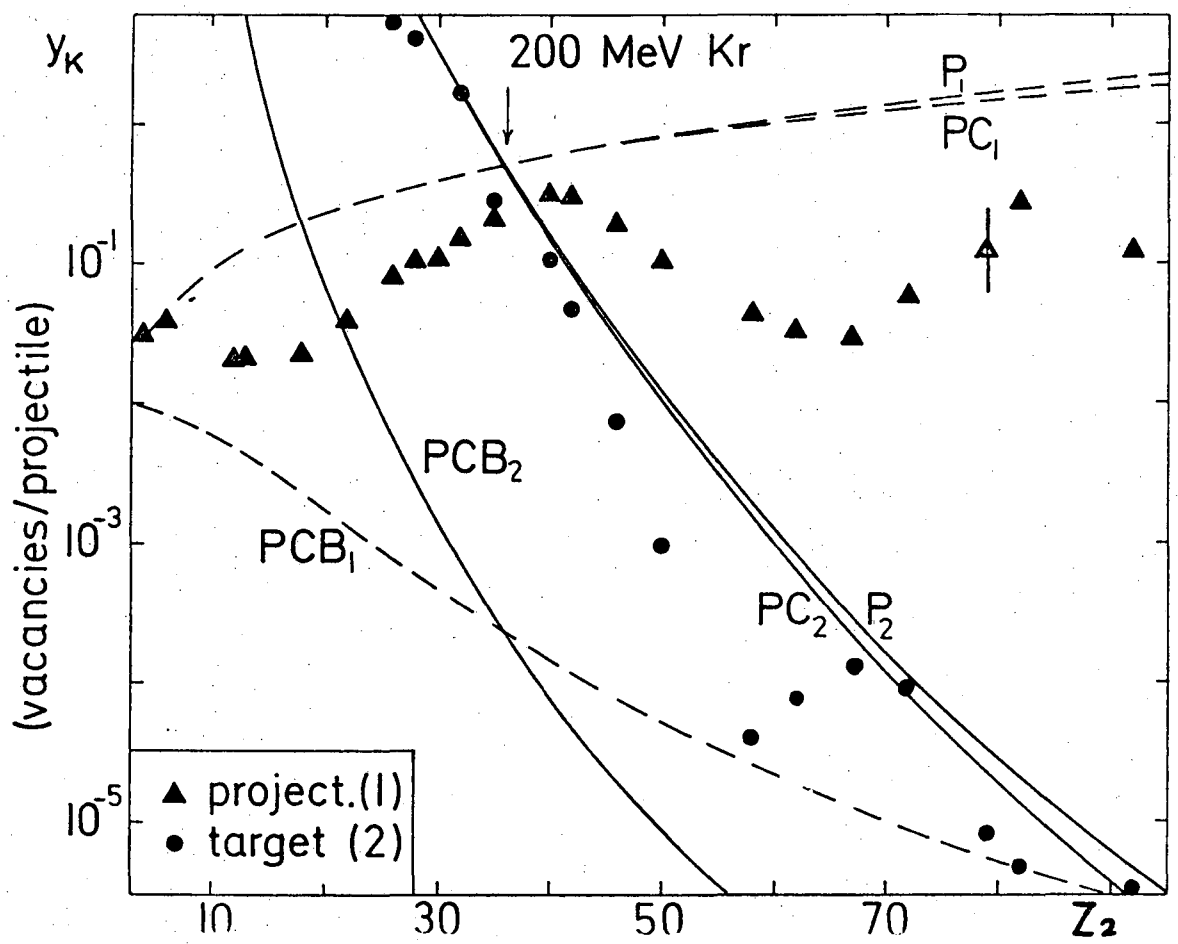

XBL 7510-8403

Fig. 6. Thick target yields for 200 MeV ^{84}Kr ions. Triangles: Kr K vacancy yields, solid circles: target K vacancy yields. Other curves explained in text. From Meyerhof *et al.*[10]

calculations. An extension of the simple PWBA has been proposed to account for Coulomb deflection of the projectile and for the fact that the 1sσ binding energy becomes larger during the collision.[4] P_1 and P_2 give the PWBA calculated cross sections for the projectile and target respectively. PC gives the PWBA result modified for Coulomb deflection and binding effects. Cross sections calculated by these models were integrated over the range of the projectile using Eq. (3.3) to obtain thick target yields. Looking at this figure, a number of points are clear. The binding energy corrections over-correct the yields, giving cross sections which are much too low. The uncorrected PWBA theories hardly fit the data at all except fortuitously near $Z_1 = Z_2$. None of these calculations predict the peak in the projectile yields observed at $Z_2 \approx 40$ and $Z_2 \approx 82$. In short, as we expect from our theoretical discussion of the PWBA, SCA, and BEA methods, the atomic model and even the corrected atomic model fails almost universally to predict cross sections in near symmetric heavy ion collisions.

Let us turn now to the molecular interpretation of the data. Figure 7 shows the same data as Fig. 6 but is divided into several regions. In region I, the 1sσ orbital correlates to the projectile 1s state and the 2pσ to the target 1s state. The dash-dot curve estimates the contribution to the projectile K x-ray yield through Demkov sharing of target K vacancies. This contribution is small so we believe that most of the projectile x-ray yield comes from direct 1sσ excitation either to the continuum or to high bound states ($\sigma_C + \sigma_{HS}$). An insignificant number of vacancies are transferred to and from the 1sσ level. The target K vacancies originate mainly from 2pσ excitation (except where $Z_2 < \frac{1}{2} Z_1$ from 3dσ excitation) and are a direct measure

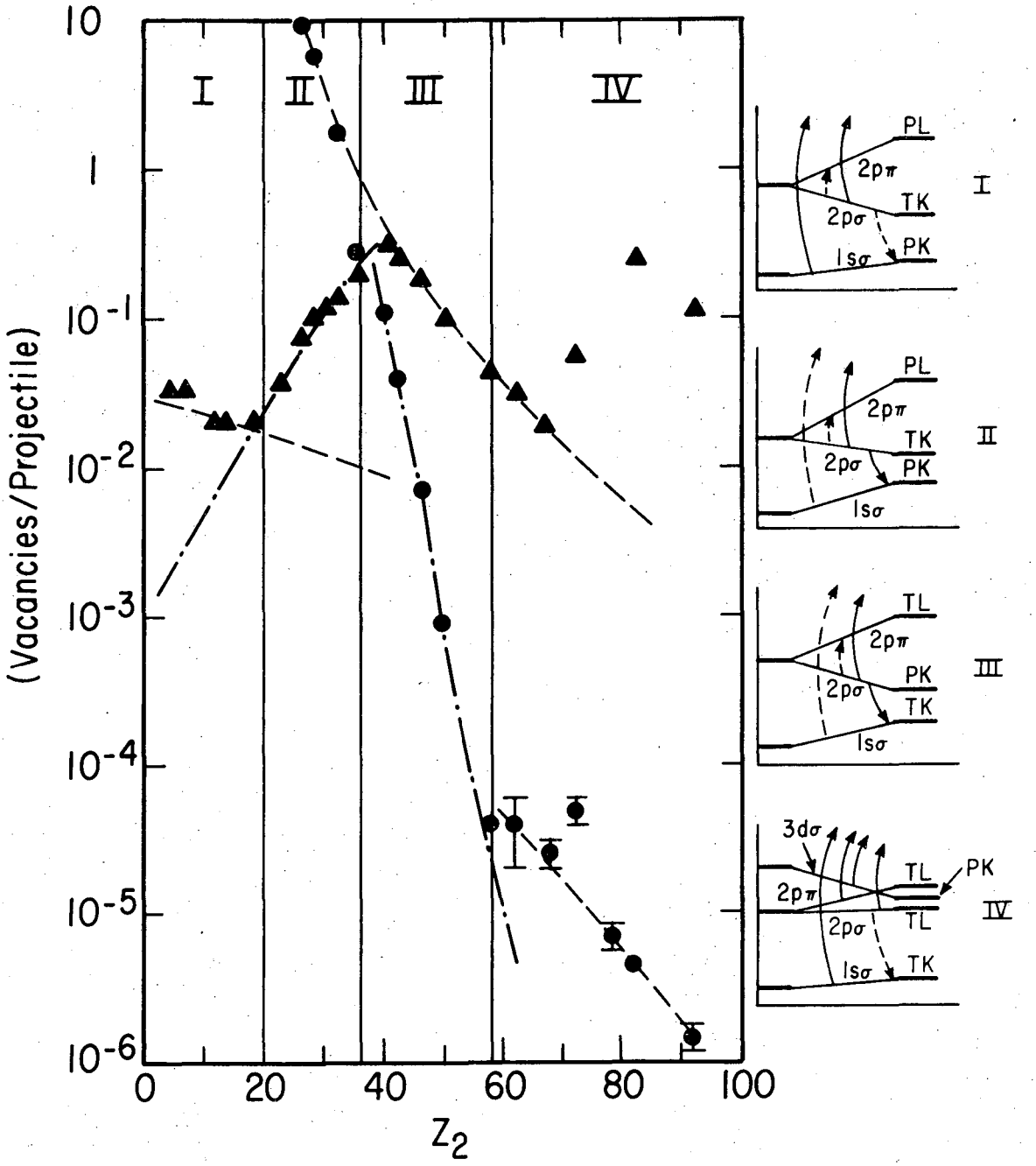

XBL 7511-8989

Fig. 7. Thick target yields for 200 MeV Kr ions. Triangles: projectile (P) K vacancy yields, circles: target (T) K vacancy yields. Dashed line gives cross section interpreted to be due to direct $2p\sigma$ and $1s\sigma$ excitation. Dash-dot line gives estimated vacancy sharing between target and projectile.

of the 2pσ cross section $\sigma_{MC} + \sigma_{MS} + \sigma_C + \sigma_{HS}$. Because there should be no vacancies in the Kr L shell, rotational transitions from the 2pσ to 2pπ orbital are not allowed in these cases except through the multi-step and multi-collision processes.

In region II, the 1sσ again correlates to the projectile K shell, and the 2pσ to the target. Here, however, the Demkov contribution from the target K shell to the projectile K yield overwhelms the direct excitation contribution. The target yield is still a measure of the 2pσ cross section except near symmetry where up to half of the 2pσ vacancies are transferred to the projectile.

In region III, the 2pσ orbital correlates to the projectile K shell and the 1sσ to the target K shell. The Demkov transition probability from the 2pσ to the target K yield overwhelms the direct 1sσ excitation in this case also. Here, the projectile K yield is a measure of the 2pσ cross section, and the target K yield is an indirect measure of the 2pσ cross section through the Demkov transition probabilities.

Finally, in region IV new effects occur. The projectile K shell becomes degenerate with the target L shell and eventually correlates to the 3dσ orbital. Therefore, the projectile yield is no longer a measure of the 2pσ cross section, but probably of the 3dσ, 2pπ, and 2sσ cross sections. We have not investigated this level matching effect and will not discuss it further.*

The target K vacancy yield observed in region IV comes from two processes: internal conversion of Coulomb excited γ-ray transitions

---

*Foster *et al*[57] have also noted this effect. Fortner[76] has discussed 3dσ excitation in Cl + C systems.

and direct 1sσ excitation to the continuum and high bound states. In Fig. 6 we show uncorrected yields; in Fig. 7, we show yields from which the γ-ray internal conversion contribution was subtracted using procedures discussed in Chapter III and Appendix A. The corrected K vacancy yield for the heavier collision partner should give a measure of the cross section for ionization and excitation of the 1sσ electron.

In Fig. 8 we show other thick target yield data measured by Meyerhof *et al.*[10] Similar conclusions about the origin of these yields in various regions can readily be made.

4.3 Scaling Laws

Meyerhof has attempted to develop scaling laws to predict the 2pσ and 1sσ cross sections obtained from this work and by other workers. We mentioned earlier that the PSS method does not provide much guidance in predicting how a cross section obtained for a certain projectile velocity and combination of Z_1 and Z_2 is related to a cross section for different velocity and combination of Z_1 and Z_2. In addition, few PSS calculations of the multi-step, ionization, and bound state excitation cross sections have been made so that no comparison between theory and experiment is possible. Using the expected scaling relations [Eqs. (2.25 - 2.27)] as a partial guide, Meyerhof has searched for general scaling laws which group all of the 2pσ and 1sσ cross sections on a single curve or two curves. The conclusions which one might reach if successful in this endeavor are a subject of considerable debate in the atomic physics community. It has been pointed out that although one can develop a scaling law that approximately predicts Pb K cross sections for p + Pb encounters as well as for Kr + Pb encounters,

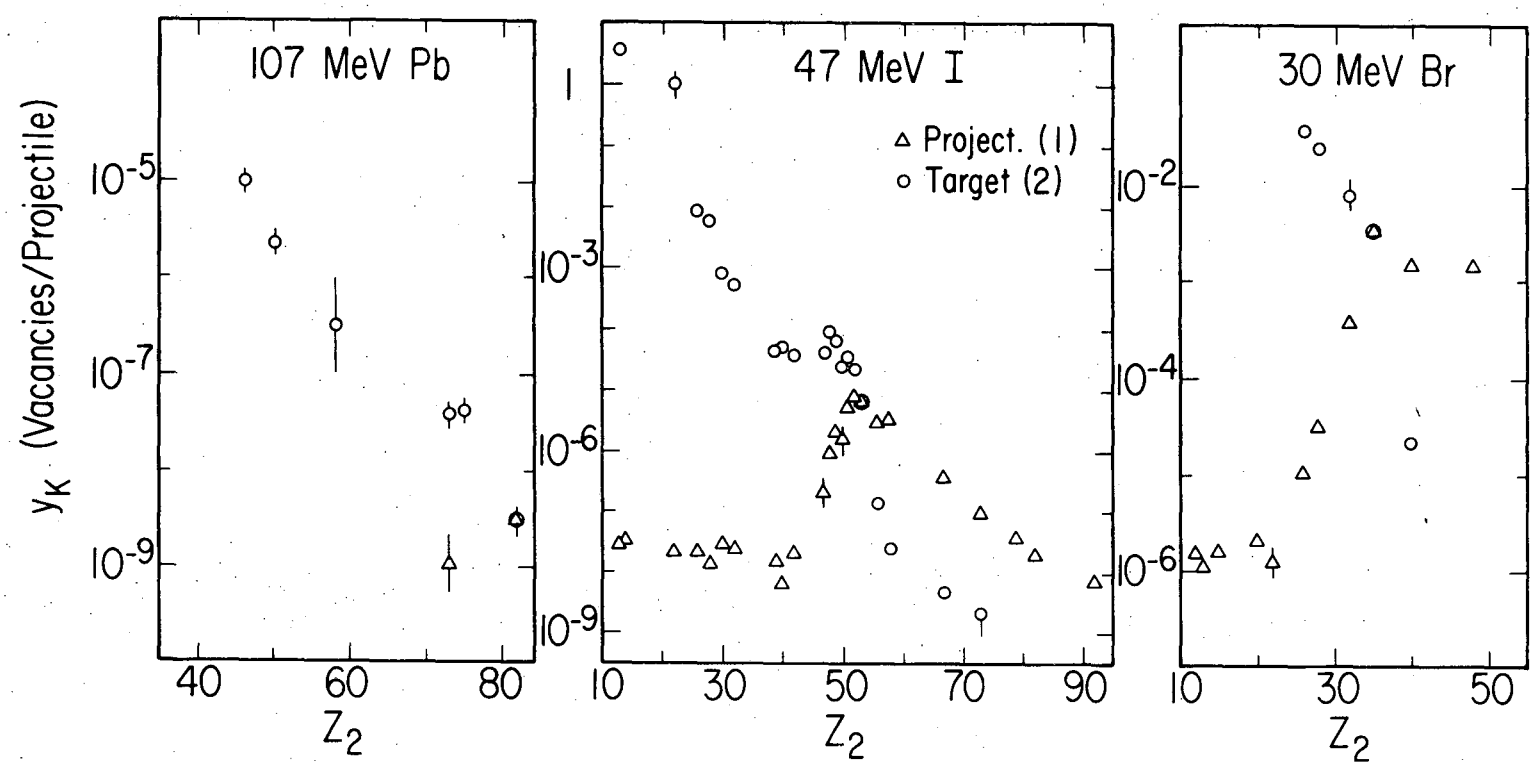

XBL 7511-8995

Fig. 8. Thick target yields using 107 MeV Pb ions, 47 MeV I ions, and 30 MeV Br ions. Triangles: projectile K vacancies, circles: target K vacancies.

this in itself does not allow the conclusion that the measured Kr + Pb cross section is necessarily due to the K shell ionization, although one knows that the p + Pb cross section is. If it turns out that these two cross sections are due to two different processes, one will be hard pressed to explain why they fit on the same curve. In any case, the curves obtained by Meyerhof group the data within a factor of ten, so there is room to introduce other scaling law curves and to explain differences in terms of other processes. At the very least, the scaling law curves have been of considerable use to us in planning experiments and in analyzing MO x-ray yields where no measured K vacancy cross sections were available.

The first scaling attempts followed what is expected from Eq. (2.25). The $2p\sigma$ and $1s\sigma$ cross sections for symmetric collisions were multiplied by Z^2 and were plotted as a function of $\eta_K = E_1/(A_1 \lambda U_K)$. The $2p\sigma$ data was obtained by measuring K vacancy cross sections in symmetric collisions. The $1s\sigma$ cross section was extrapolated from very asymmetric collisions assuming that for $Z_1 > Z_2$ the projectile cross section or thick target yield is the $1s\sigma$ cross section and is a smoothly decreasing function of Z_2. For Kr, there are few points on which to base such an extrapolation. A rough extrapolation would follow the straight line shown in Fig. 7. Better examples can be found in Meyerhof's 30 MeV Br work and especially in the 47 MeV I work shown in Fig. 8. Figure 9 shows the resulting scaled data and compares with theoretical predictions of p + H ionization cross sections made by Thorson *et al.*[19] (The theoretical curves are misplotted here. They should lie a factor of two higher in energy or a factor of 16 lower in cross section. For reasons which will be discussed later, the

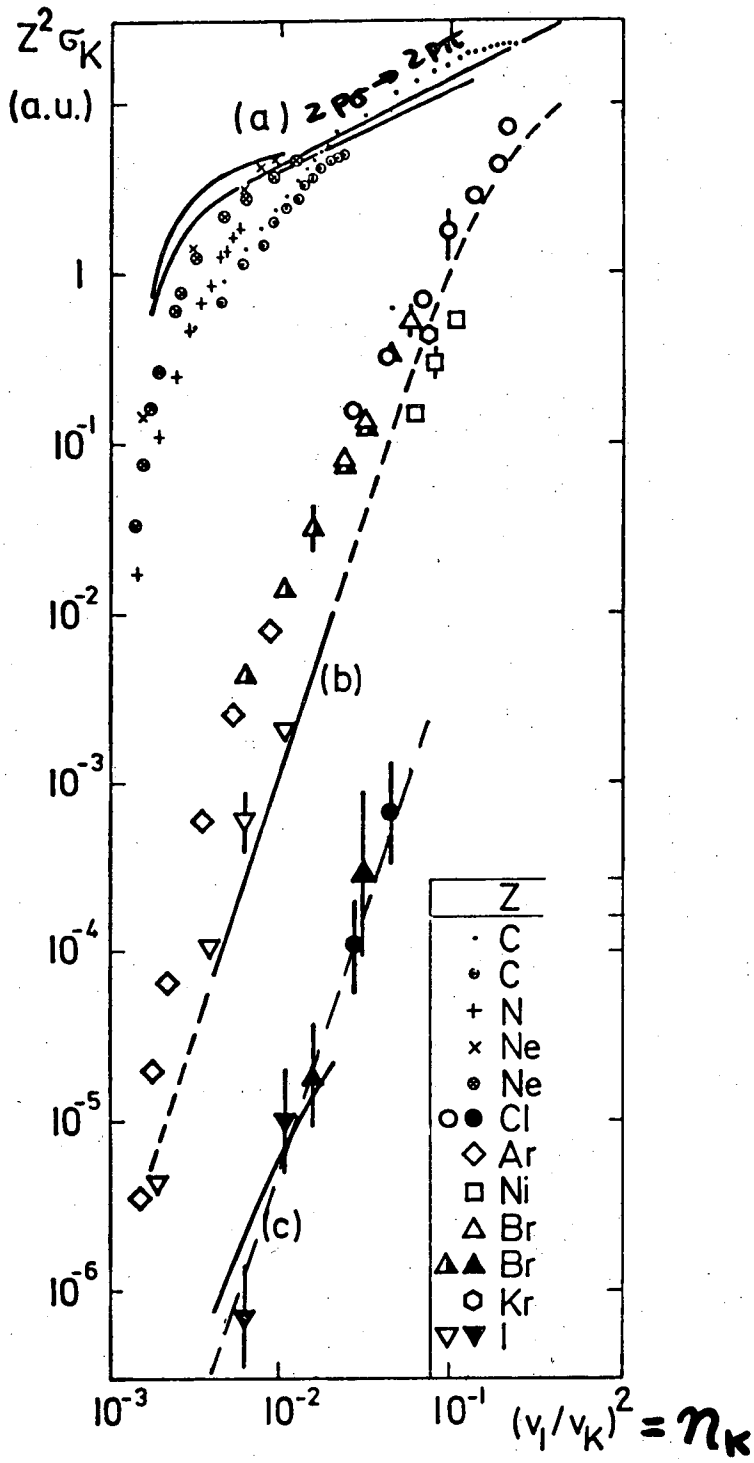

XBL 7510-8399

Fig. 9. Scaled K-vacancy-production cross sections for symmetric ion-atom collisions versus reduced projectile energy. Curves (a): Theoretical calculations for 2pσ-2pπ rotational coupling transitions,[9] curves (b) and (c): Theoretical calculation for 2pσ and 1sσ ionization.[19] Dashed curve drawn to guide eye. Taken from Meyerhof.[53]

calculated 1sσ cross section is over estimated by orders of magnitude.)

The grouping of the data long curves (b) and (c) led Meyerhof[53] to the assumption that the groups represented the 2pσ and 1sσ excitation cross sections, respectively. However, the Pb + Pb cross section later measured using 87 and 107 MeV Pb ions[55] was found to lie two orders of magnitude lower than the trend of the 2pσ group to which those cross sections should belong. A possible explanation for this discrepancy is that in Pb + Pb collisions the 2pσ (or $2p_{1/2}$) orbital, instead of being promoted to a lower binding energy near the UA limit, actually correlates to much higher binding energy near the UA. Figure 10 illustrates this effect for U + U collisions.[54] The diagram for Pb + Pb encounters is similar. Since a larger energy transfer is required to eject the 2pσ electron into the continuum in Pb + Pb encounters, the cross section is correspondingly smaller.

This suggested a possible modification of the 2pσ scaling law by using the binding energy G of the 2pσ electron at the distance of closest approach instead of the SA binding energy to calculate η_K. The binding energy at the distance of closest approach was proposed, rather than the UA binding energy, because for insufficient bombarding energy the UA limit cannot be reached. This proposal takes Coulomb repulsion into account in a very crude manner. The idea also follows from theoretical work of Basbas *et al.*[73] For most of the medium-Z elements this would cause practically no change from the previous scaling law since in symmetric collisions the $2p_{1/2}$ binding energy is nearly identical to the SA K binding energy. For the heavy elements, however, a major change is made in the scaling. Plotting the 2pσ cross section for symmetrical collisions multiplied by Z^2 versus the

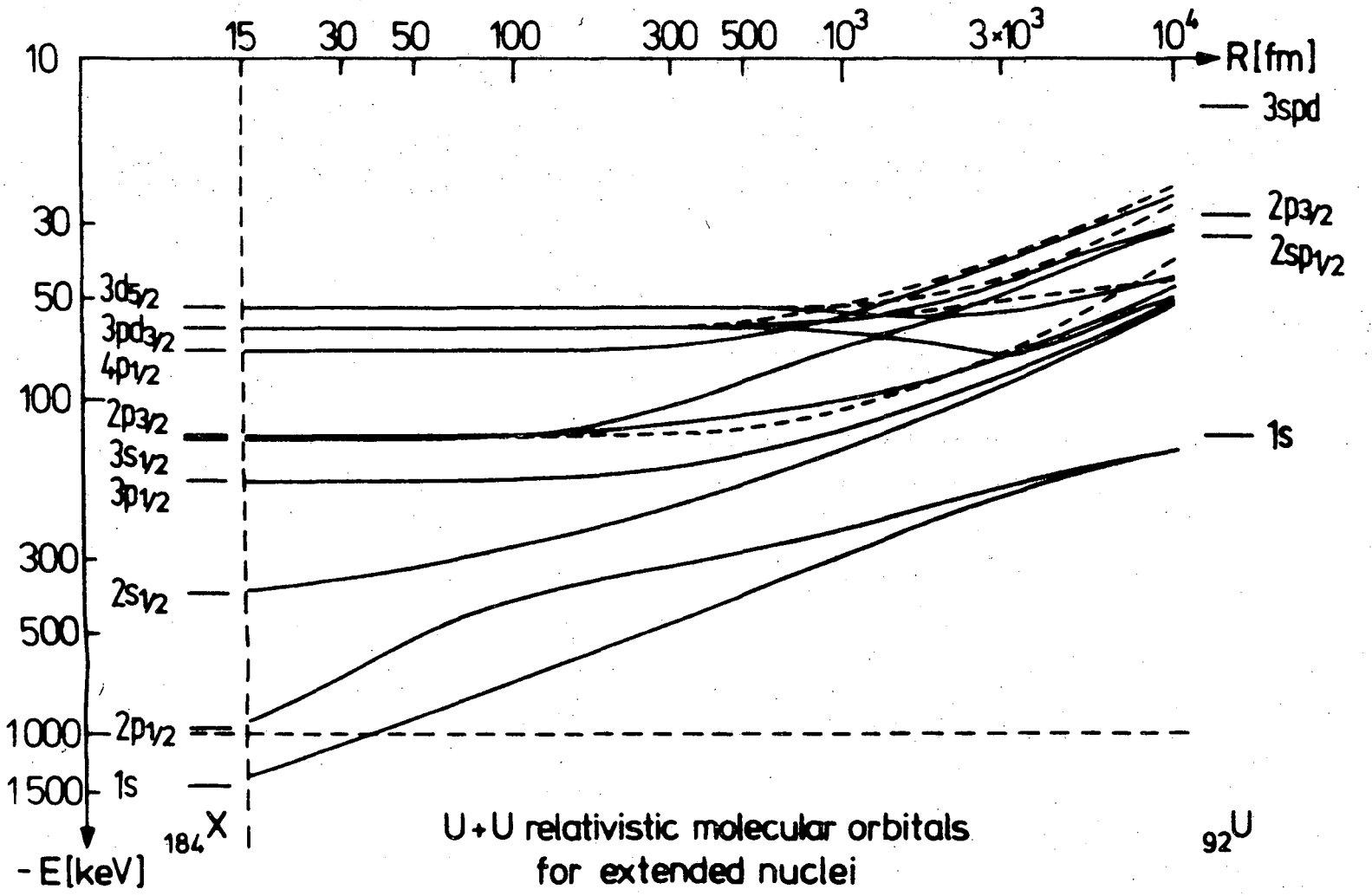

Fig. 10. Correlation diagram for U + U encounters (from Müller[54]). The $2p_{1/2}$ orbital correlates to a much higher binding energy in the UA limit than in lighter projectile-target systems (e.g., Ar + Ar, shown in Fig. 1).

XBL 7510-8400

new parameter, the curve shown in Fig. 11 was obtained. Here, for $Z < 50$, only cross section data taken using gas targets is included. In these cases the contribution from the multi-collision process is expected to be negligible. Attempts to extend this scaling law to asymmetric collisions have not been as successful, as Fig. 12 shows. Both solid target data and gas target data are present there. An expression for Z_{eff} was obtained empirically and the choice giving the best results is:

$$Z_{eff}^{-1} = \frac{1}{2}\left[Z_1^{-1} + Z_2^{-1}\right] \tag{4.8}$$

With the choice of Z_{eff} given by Eq. (4.8) the experimental $1s\sigma$ cross sections were found not to scale with the energy gap at the distance of closest approach. Instead, Meyerhof found that the $1s\sigma$ cross section data obeys a SA energy gap scaling law similar to what was previously proposed. For asymmetric encounters, the SA binding energy of the higher-Z collision partner was chosen to calculate $\eta_K = mE_1/(M_1 U_K(H))$ [similar to Eq. (2.2)]. In addition, η_K should be multiplied by $\frac{1}{4}(1 + Z_L/Z_H)^2$ where Z_L and Z_H are the lower and higher atomic numbers of the projectile or target. Figure 13 shows $1s\sigma$ cross section data plotted using this modified scaling parameter and Z_{eff} given by Eq. (4.8). The data is closely grouped around the dashed line in this figure. The equation for the dashed curve is

$$Z_{eff}^2 \sigma = 7770\left[\frac{mE_1}{MU_K(H)} \times \frac{1}{4}\left(1 + \frac{Z_L}{Z_H}\right)^2\right]^{4.3} \text{a.u.} \tag{4.9}$$

and can be used to obtain cross sections reliable to about a factor of five.

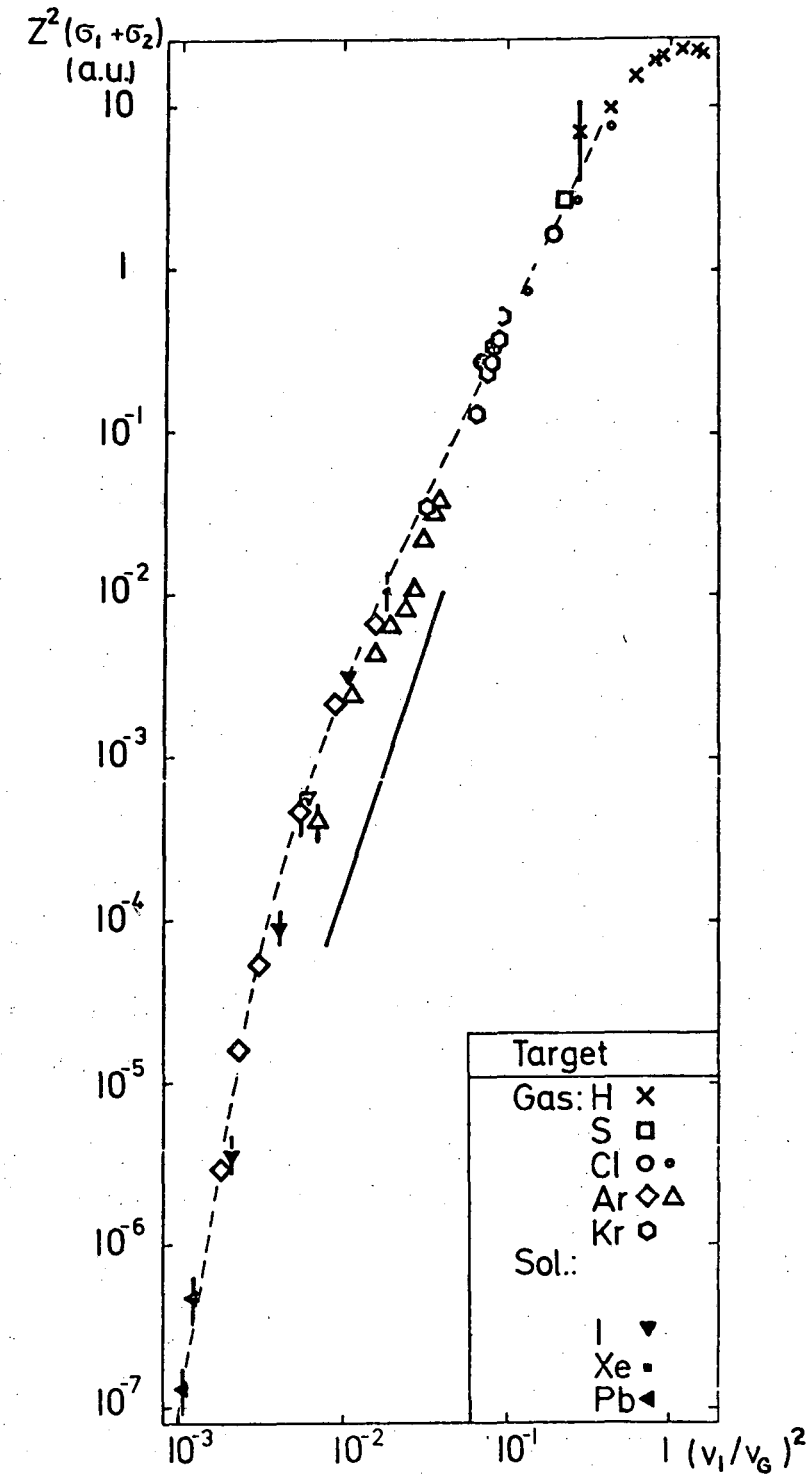

XBL 7510-8401

Fig. 11. Scaled 2pσ cross sections (sum of projectile and target K vacancy cross sections) versus new reduced projectile energy. v_G is defined from the 2pσ energy gap at the distance of closest approach between the projectile and target nuclei. Taken from Meyerhof *et al.*[10]

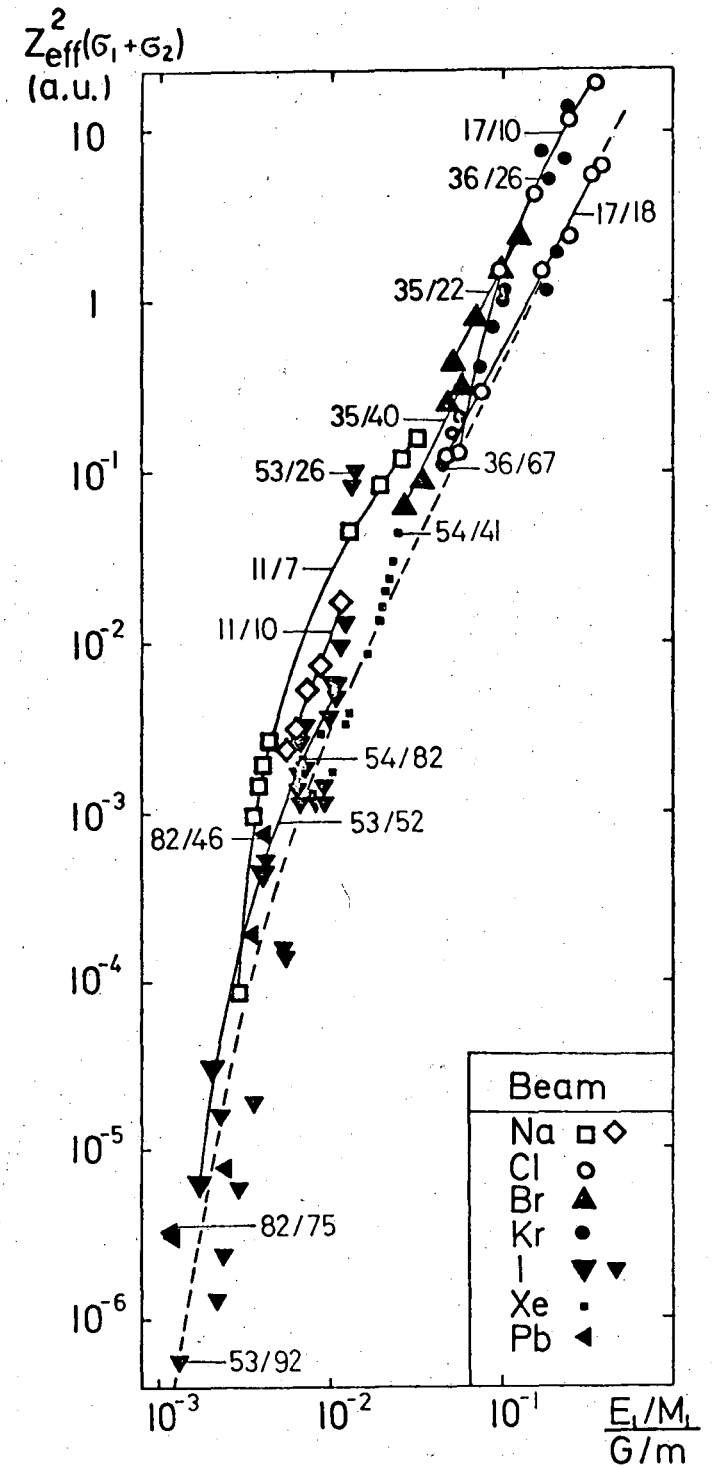

XBL 7510-8398

Fig. 12. Scaled 2pσ cross sections for asymmetric collisions only with Z_{eff} given by Eq. (4.8). Certain measurements are marked by the ratio of Z_1/Z_2. Dashed curve was taken from approximate fit to data shown in Fig. 10. Solid lines connect cross sections measured as a function of projectile energy. Taken from ref. 10.

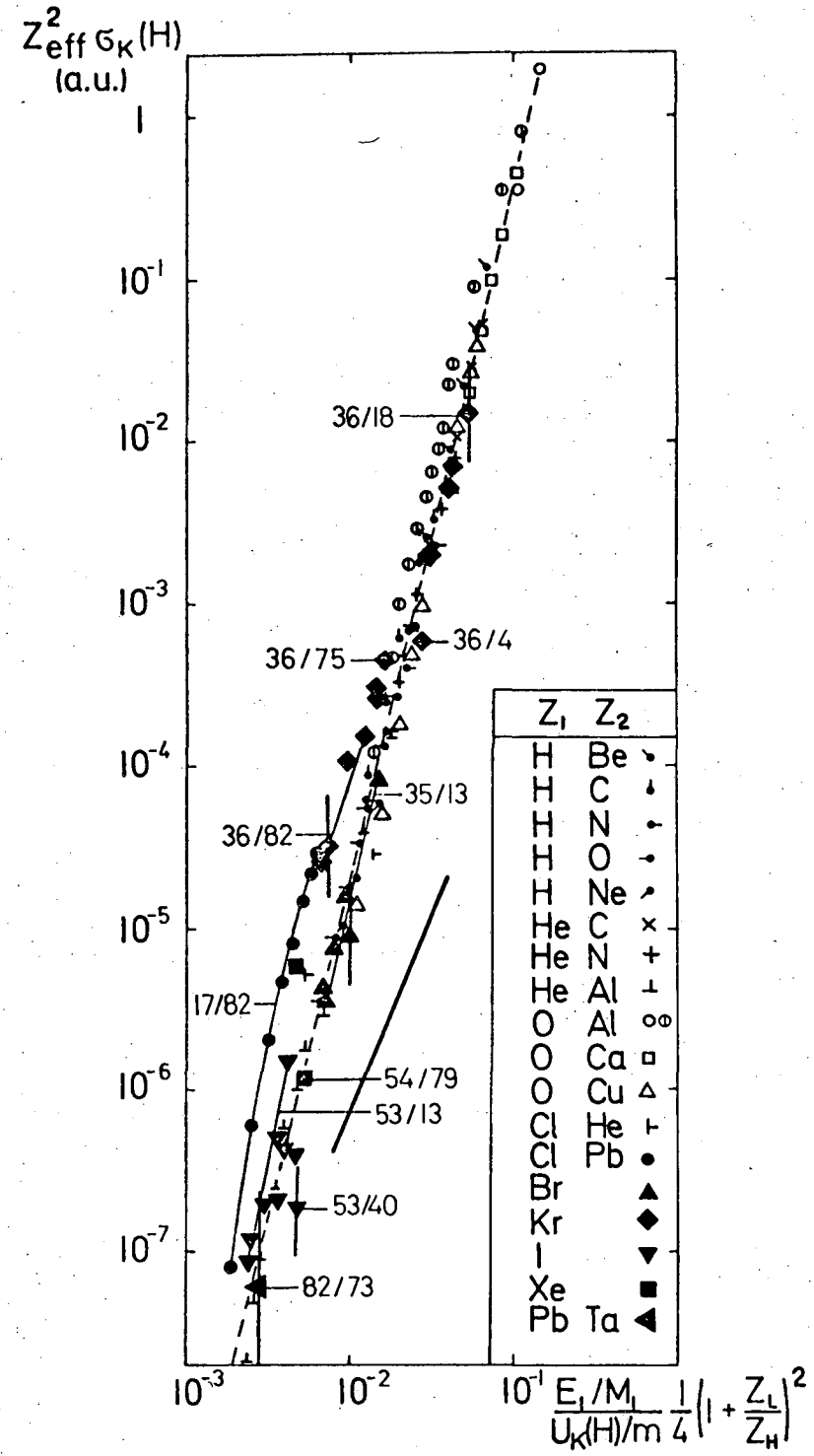

Fig. 13. Scaled 1sσ vacancy production cross sections observed as K x rays in the heavier collision partner in very asymmetric collisions with Z_{eff} given by Eq. (4.8). Selected values of Z_1/Z_2 are shown. Light solid lines connect certain cross sections measured as a function of bombarding energy. The heavy solid line gives the theoretical 1sσ ionization cross section computed by Thorson *et al.*[19] Dashed lines shows a $E_1^{4.3}$ dependence which best fits the data. Taken from Meyerhof *et al.*[10]

Another scaling law attempt was made recently by Foster *et al.*[57] As previously proposed by Hansen,[26] they suggested that the cross sections should be scaled by the UA binding energy and compared this scaling law to the BEA theory. In the BEA theory, the cross section is written as

$$\sigma U_K^2 / Z_1^2 = f(E_1/\lambda U_K) \tag{4.10}$$

where E_1 is the projectile energy, λ is the ratio of the electron mass to the projectile mass, and U_K is the binding energy of the higher-Z collision partner. Foster *et al*[57] proposed that the SA binding energy should be replaced by the UA binding energy and that Z_1 should be replaced by Z_{eff}, where Z_{eff} is $[(Z_1^2 + Z_2^2)/2]^{\frac{1}{2}}$ for $2p\sigma$ cross sections or Z_1 for $1s\sigma$ cross sections. We call this modification the UABEA scaling law. Both the $2p\sigma$ and $1s\sigma$ cross sections should fall along a single curve which is given by the BEA f function. Figure 14 compares the familiar BEA scaling law with the UABEA law. The open points in these figures are $1s\sigma$ cross section data and the closed points are $2p\sigma$ cross section data. The UABEA modification clearly groups both the $2p\sigma$ and $1s\sigma$ cross section data closely around the universal curve and therefore is a successful scaling relation. We shall return to discuss this scaling law in a later chapter where we will attempt to apply it to our Kr data.

Scaling laws indicate how the $2p\sigma$ and $1s\sigma$ cross sections might vary as a function of projectile energy, Z_1, and Z_2, and for that reason are useful. However, their usefulness in resolving certain questions is limited. For instance, Meyerhof's scaling law for the $1s\sigma$ cross section uses a SA energy gap, but Foster *et al*[57] use the UA energy gap.

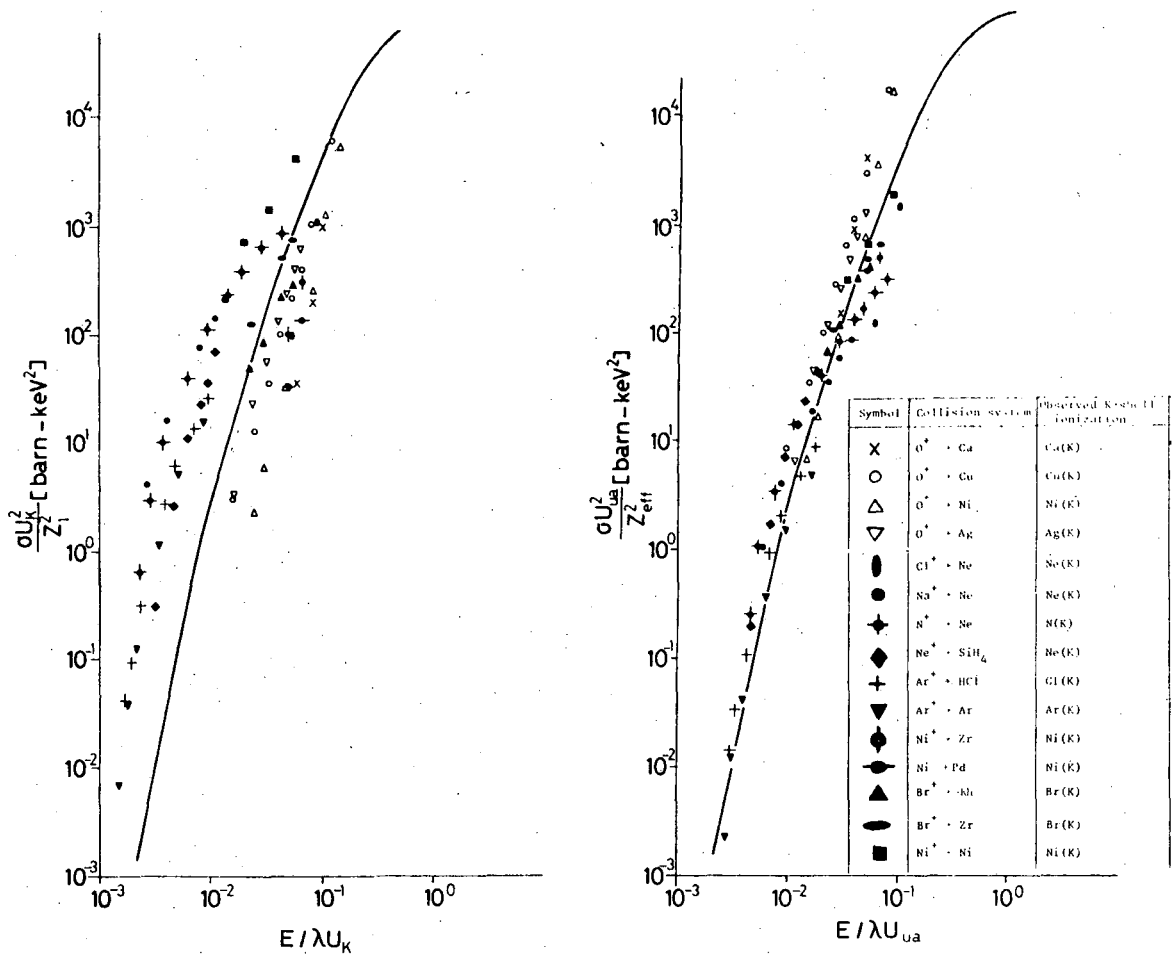

XBL 7512-9766

Fig. 14. Scaled 1sσ (open symbols) and 2pσ (closed symbols) cross sections versus reduced projectile energy. Left is a plot of the data using the BEA relations. Right: the UABEA scaling law. The SA binding energy is replaced with the UA binding energy and Z_{eff} is $\left((Z_1^2 + Z_2^2)/2\right)^{\frac{1}{2}}$ for 2pσ cross sections or Z_1 for 1sσ cross sections. From Foster *et al.*[57]

Is the 1sσ cross section data displayed in Fig. 13 grouped more closely than the data displayed in Fig. 14? Does that indicate that the 1sσ cross section depends on the SA energy gap instead of the UA energy gap? The answers to these questions probably cannot be obtained from Figs. 13 and 14, but can only be obtained by a more careful examination of cross sections obtained by varying only a limited number of experimental parameters. For instance, while keeping the projectile velocity constant and a measurement of 1sσ or Kr K vacancy cross sections in encounters with H, He, Li, ... and Cl projectiles might indicate whether the cross section decreases with the UA binding energy or not. Plotting cross sections on universal scaling plots is an insensitive tool in examining how cross sections vary with different combinations of Z_1 and Z_2.

V. THEORY OF 1sσ EXCITATION

Little theoretical work has been doen to calculate the cross section for the ejection of 1sσ electrons into the continuum for a wide variety of collision partners. Both the 2pσ and the 1sσ ionization cross sections were previously calculated for 200 to 1000 eV H^+ + H encounters by Thorson and co-workers[19] using the method of PSS. While their formulation of the problem is essentially correct, their calculations of these quantities were in serious numerical error. Hence their values of the two cross sections cannot be trusted.

Unfortunately, Thorson's calculations can only be applied to symmetric collisions where the 1sσ ionization cross section is unmeasurable. Calculations are therefore needed for asymmetric collisions where direct comparisons with 1sσ cross section data is possible. An approach taken by Basbas and co-workers[4] was to begin with very asymmetric encounters where the PWBA, BEA, and SCA theories are applicable and to modify those results to account for the Coulomb deflection of the particle and the fact that the binding energy of the 1sσ electron does not stay constant, but correlates to the UA binding energy during the collisions.

We have attempted to use both of these methods to calculate 1sσ ionization cross sections and I discuss that work in this chapter. Lastly, I give estimates of the contribution to the total K-vacancy yield due to excitation of 1sσ electrons to high bound states.

5.1 Model Calculations for p + H Collisions

Calculations of the total 1sσ ionization cross section for symmetric encounters, the impact parameter dependence of the 1sσ

ionization probability, and the cross section differential in the final electron kinetic energy are described in Appendix B. The amplitude for excitation of a 1sσ electron into a continuum state having energy ε and quantum numbers i,j, ... (specified in Appendix B) is

$$a(i,j\ldots\varepsilon,b,E_1,\infty) = \int_{-\infty}^{\infty} dt\, M(ij\ldots\varepsilon, R(t))\, e^{i\int_{-\infty}^{t}(\omega_{1s\sigma}(R(t'))-\varepsilon)\,dt'} \tag{5.1}$$

where M is the matrix element of the radial or rotational coupling operator connecting the 1sσ state to the continuum state (i,j, ... ε) and the time integral is over a Rutherford trajectory with impact parameter b and ion energy E_1 [see also Eq. (2.19) and Eq. (B.3)]. For our model calculations, we use a simple parameterization of the 1sσ energy gap $\hbar\omega_{1s\sigma}(R)$. We fitted matrix elements calculated by Thorson and co-workers[19] to simple analytical functions and evaluated trajectory integrals using these simple functions. In this Section, we report on the cross section differential in final kinetic energy dσ/dε, the impact parameter probability P(b,E), and the total cross section $\sigma_{1s\sigma}(E)$ defined as

$$\frac{dP}{d\varepsilon}(\varepsilon,b,E_1) = \sum_{i,j,\ldots} |a(ij,\ldots\varepsilon,b,E_1,\infty)|^2$$

$$P(b,E_1) = \int_0^{\infty} d\varepsilon\, \frac{dP}{d\varepsilon} \tag{5.2}$$

$$\frac{d\sigma}{d\varepsilon}(\varepsilon,E_1) = \int_0^{\infty} 2\pi b\,db\, \frac{dP}{d\varepsilon}$$

$$\sigma(E_1) = \int_0^{\infty} \frac{d\sigma}{d\varepsilon}\, d\varepsilon \text{ or } \int_0^{\infty} 2\pi b\,db\, P(b,E_1)$$

5.1.1 The total cross section

Figure 15 shows the total 1sσ ionization cross section obtained in this calculation and compares with "experiment" and with similar calculations made using constant energy gaps $\hbar\omega_{1s\sigma}$ = 0.5, 1.0, 1.5, and 2.0 a.u.. Since the 1sσ ionization cross section cannot be measured in symmetric collisions [see discussion following Eq. (4.3)], the experimental cross section has to be inferred from very asymmetric encounters. The curve shown in Fig. 15 is based on Meyerhof's SA energy gap scaling law[10] (Fig. 13). We shall compare with experiment in later chapters.

Rather than emphasizing the comparison with experiment in this chapter, we shall emphasize the comparison with cross sections calculated using a constant energy gap, the dashed curves in Fig. 15. In p + H encounters, the SA binding energy is 0.5 a.u., but the UA binding energy is 2.0 a.u.. The figure shows that the calculation using the UA energy gap comes closest to reproducing our calculation which uses a good approximation to the actual R dependence of the 1sσ energy gap for H_2^+.

The fact that the 1sσ energy gap is 0.5 a.u. at infinite internuclear separation and increases to 2.0 a.u. in head-on collisions as $R \to 0$ does not seem to be important in these low velocity collisions. The cross section depends just on the UA energy gap, suggesting that excitation occurs at short internuclear distances during the collision. In developing the SA energy gap scaling law for 1sσ excitation, Meyerhof pointed out that it is most likely for transitions from the 1sσ orbital to the continuum to occur at large internuclear distances because less energy transfer is required there. A smaller

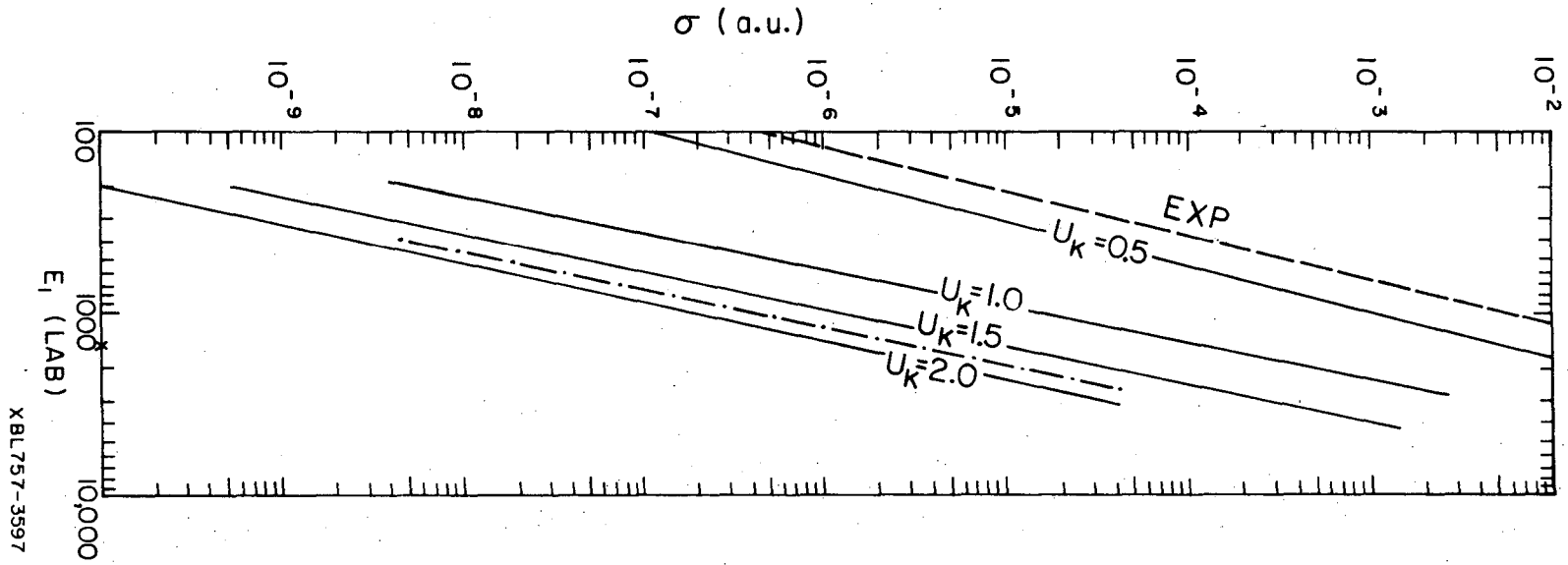

Fig. 15. Cross section for 1sσ ionization in a.u. (2.79×10^{-17} cm^2) versus proton lab energy in eV for p + H collisions. Dashed line: "experimental" 1sσ ionization cross section based on Meyerhof's scaling law. Dash-dot: calculated 1sσ cross section using model outlined in Appendix B. Solid curves are based on same model except that a constant energy gap of 0.5, 1.0, 1.5, and 2.0 a.u. was used.

0 0 1 0 4 4 0 3 3 4 6

energy transfer implies a greater probability that ionization will occur. Nevertheless, the implications of our calculation are that excitation occurs at very close internuclear distances, surprisingly, where a greater energy transfer is required.

We would like to suggest two arguments why transitions necessarily must occur at short internuclear distances. Consider the classical BEA† view of K shell ionization and recall our arguments showing that for ionization of a K electron in, for example, a 30 MeV Br + Br collision, the initial electron kinetic energy must be at least 60 keV or four times its average binding energy. In the Bohr atom picture, the kinetic energy of the K electron is classically related to its orbiting radius about the target nucleus through Eq. (2.15). Large kinetic energies imply that the electron must be orbiting close to the target nucleus, therefore the projectile must strike the K electron at close distances to the target nucleus to be ionized. The fact that less energy transfer is required at larger internuclear distances is not relevant when the projectile by itself does not provide sufficient momentum transfer to ionize the K electron. Excitation must occur at close internuclear distances, therefore, an energy at least as large as the UA binding energy must be transferred to the $1s\sigma$ electron.

Another argument can be made if we make the connection between the impact parameter dependence of $1s\sigma$ ionization and the R dependence of $1s\sigma$ ionization along a given trajectory. In the SCA theory[17] of

---

†I am grateful to J. D. Garcia who stimulated this argument.

K-shell ionization by light projectiles, P(b) decreases as

$$P(b) \sim e^{-b/a} \tag{5.3}$$

with $a = a_K v_1/v_K$. The fall-off parameter a may be viewed as a "radius of excitation". Excitation occurs when the projectile is within this radius. Outside of that radius, the excitation probability is small. The excitation probability consequently depends on the energy gap inside this radius. When v_1/v_K is small, it will depend on the UA energy gap. Only when v_1/v_K is very large will excitation depend on the SA energy gap.

These arguments are based on atomic models, in the former case the BEA theory, in the latter the SCA theory, and their application to molecular encounters is not rigorously justified. We have made them in an attempt to show physically why our p + H 1sσ cross sections display the UA energy gap dependence. Using the method of PSS, Basbas, Brandt, and Ritchie[73] have developed an argument to justify the use of the binding energy at the distance of closest approach in place of $\omega_{1s\sigma}(R)$ in Eq. (5.1). Their argument is very formalistic, however, and provides little physical insight into why such an approach is correct. In addition, their derivation is very involved and for this reason I shall not attempt to repeat it here.

In conclusion, our calculations show that the 1sσ ionization cross sections may be obtained using a constant energy gap in place of $\omega_{1s\sigma}(R)$. The calculations made using the R-dependent, one-electron 1sσ energy gap agree with calculations made using constant energy gaps between 1.7 and 1.9 a.u.. We do not understand why the hydrogenic energy gap calculation does not agree exactly with a constant energy

gap calculation using 2.0 a.u., the UA energy gap. Perhaps this indicates that, following Basbas *et al*[4,73] we should use the energy gap at the distance of closest approach. Our model calculations are very uncertain, however, and drawing conclusions from the lack of exact agreement cannot be justified at this time.

5.1.2 P(b,E)

Figure 16 shows calculated values of P(b,E) obtained in this work. For these velocities P(b) is peaked at very small impact parameters and shows smoothly decreasing tails at large impact parameters. The shape of P(b) is similar to what is predicted by the SCA theory[17] for 600 - 2500 eV p + H collisions. It is in marked contrast, however, to the jagged diffraction pattern[11] behavior of P(b) previously reported by Thorson and co-workers (see ref. 19, paper V and Fig. 26) and now believed to be due to numerical errors.

For large impact parameters, P(b) clearly has a velocity dependent fall-off parameter. We fitted the exponential portions of these curves to the form given by Eq. (5.3), and divided the fall-off parameter a by v_1/v_K to obtain an approximately velocity-independent $a_0 = a/(v_1/v_K)$. Between 600 and 2500 eV, the value of a_0 varied from 0.45 to 0.606.

The simple SCA theory predicts that the value of a_0 should be $\hbar v_1/2U_K$ or that a_0 should be $a_K\sqrt{\theta_K}$. In this case $\theta_K = 1$. In practice, however, a_0 is rarely this simple, for 2500 eV p + H collisions we used the SCA theory of Brandt *et al*[89] (without Coulomb deflection and binding correction terms) to calculate P(b) and repeated the fitting procedure obtaining $a_0 = 1.23\ a_K$.

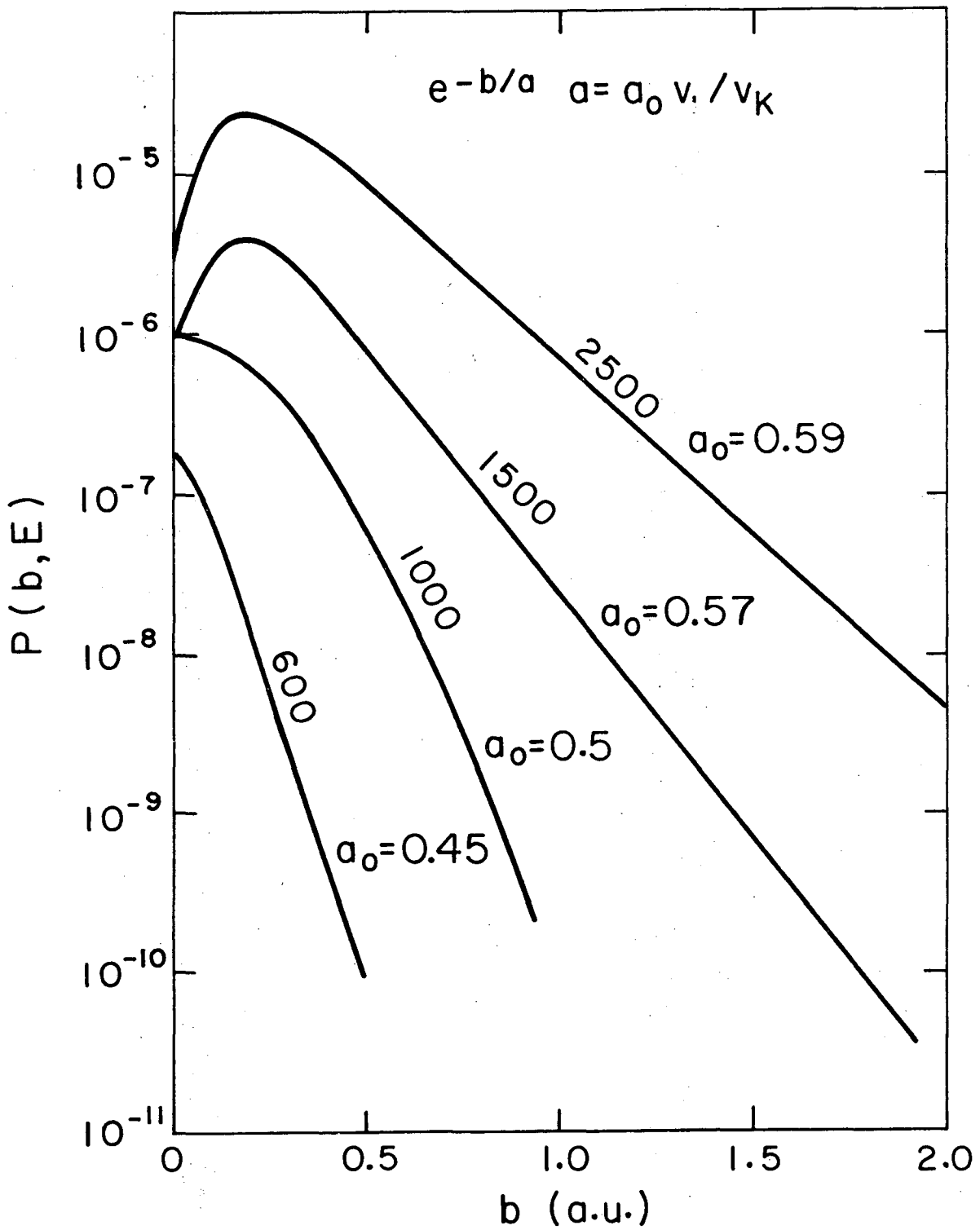

XBL757-3595

Fig. 16. Impact parameter dependence of total K vacancy production probability for 600 - 2500 eV p + H collisions.

The value of a expected for symmetric collisions could be $\hbar v_1/2U_{UA}$, consistent with the conclusion of the last section, that we can calculate the cross section by replacing the time dependent energy gap with a constant energy gap equal to approximately U_{UA}. This would give $a_0 = 0.25\ a_K$. The a_0 parameters displayed in Fig. 16 are smaller than a_K but are not as small as $0.25\ a_K$. However, since the SCA theory does not exactly predict that $a_0 = a_K$ when more accurate calculations are done, the fact that the a_0 parameters are larger in Fig. 16 cannot be taken seriously.

5.1.3 The differential cross section

The first order SCA[17] (and the PWBA[14]) for light projectile-heavy target encounters predict that the differential cross section for monopole excitations can be written approximately as:

$$\frac{d\sigma}{d\varepsilon} \approx \frac{2^{20}}{5} \frac{Z_1^2 a_K^2}{Z_2^{*2}} \eta_K^4 \frac{U_S^9}{(U_K+\varepsilon)^{10}} \tag{5.6}$$

where $4\eta_K = (2v_1/v_K)^2 << 1$, a_K is the target K shell radius, and U_S is the ideal or Slater-rule binding energy [see Eq. (2.2)]. This is called Huus' approximation. It was originally derived from the PWBA,[65] and was also derived from the SCA by Bang and Hansteen.[17]

Huus' approximation predicts that the cross section differential in final electron kinetic energy should drop off as $(U_K + \varepsilon)^{-t}$ with $t = 10$. All our previous work indicates that the UA energy gap should replace the SA energy gap in our equations, thus $d\sigma/d\varepsilon$ should drop off as a power of $(U_{UA} + \varepsilon)$. Therefore a fully logarithmic plot of $d\sigma/d\varepsilon$ versus $(U_{UA} + \varepsilon)$ should give a straight line. Figure 17 shows $d\sigma/d\varepsilon$ plotted versus ε, $\varepsilon + U_K$, and $\varepsilon + U_{UA}$. Plotting $d\sigma/d\varepsilon$ versus

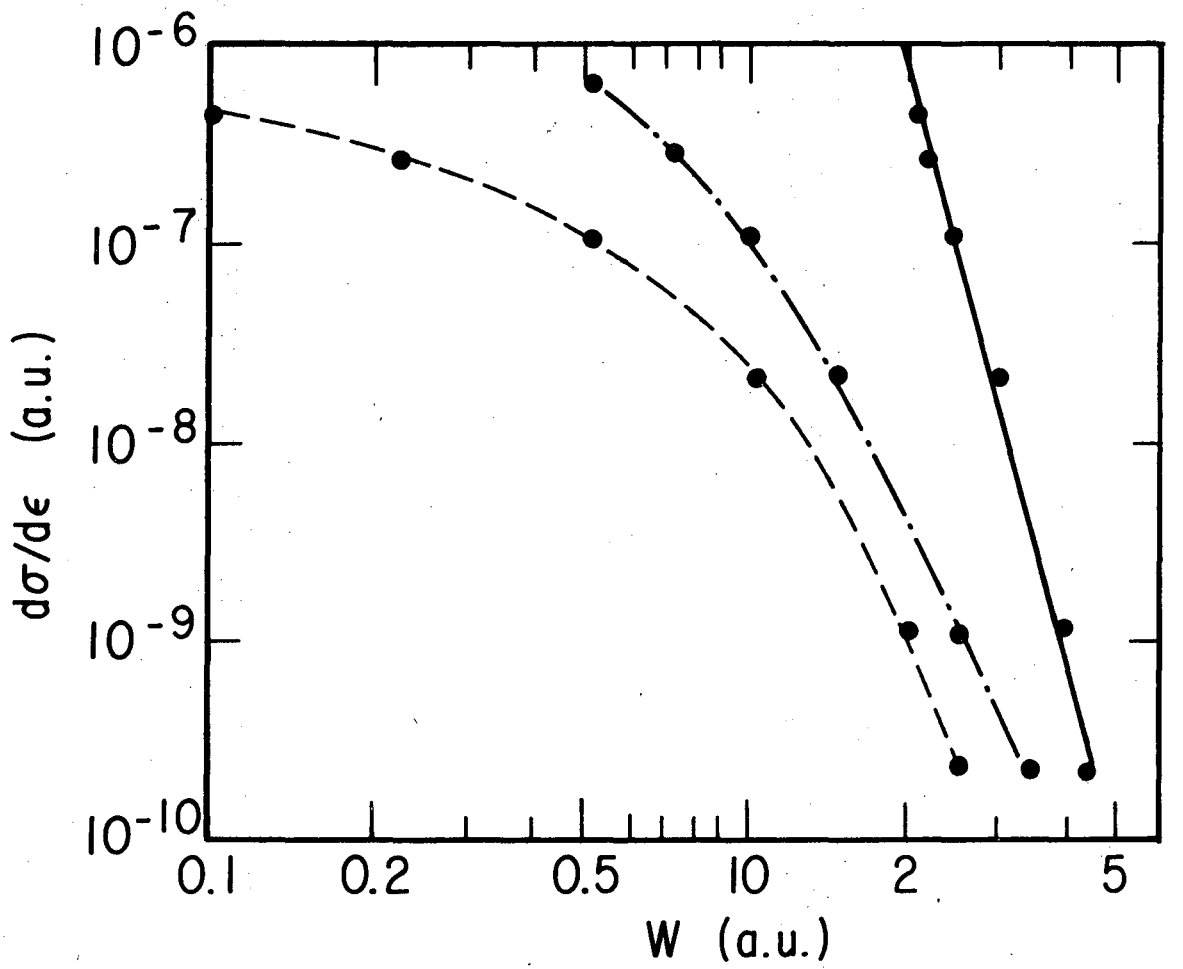

XBL 7511-8992

Fig. 17. Differential cross section in a.u. (1.02×10^{-18} cm^2/eV) for 600 eV p + H encounters versus W, where W is the outgoing electron kinetic energy ε (dashed), $\varepsilon + U_K$ (dash-dot) or $\varepsilon + U_{UA}$ (solid). The solid line gives a fit $d\sigma/d\varepsilon \sim [\varepsilon + U_{UA}]^{-t}$ with $t \approx 9.8$.

$(U_{UA} + \varepsilon)$ clearly comes closest to giving a straight line. It is interesting that t turns out to be 9.8, in close agreement with Huus' approximation.

5.2. The Binding Energy Correction

Our calculations show that to calculate the amplitude for ionization we can replace the time dependence of $\hbar\omega_{1s\sigma}(R)$ by a constant energy gap equal to U_{UA}. Basbas, Brandt, and Laubert[4] (hereafter referred to as BBL) have previously attempted to account for this dependence in their development of the binding energy correction to the PWBA. Their PSS calculation[73] indicates that it is possible to account for the amplitude for ionization by replacing $\omega_{1s\sigma}(R)$ by $\omega_{1s\sigma}(R_0)$, where R_0 is the distance of closest approach in a collision with impact parameter b and ion energy E_1. The amplitude for ionization may therefore be written as:

$$a(ij..\varepsilon, b, E_1, \infty) = \int_{-\infty}^{\infty} dt\, M(ij..\varepsilon, R(t))\, e^{i(\omega_{1s\sigma}(R_0)-\varepsilon)t} \tag{5.7}$$

Although the energy gap is a molecular energy gap, SA wavefunctions are used to calculate M. Potential coupling is assumed, and matrix elements of the projectile's Coulomb field are calculated as in Eq. (2.4). The i,j, ... quantum numbers for the final electron continuum state are LM quantum numbers in the lab frame (z axis along $\vec{v}_1$).

One can evaluate this expression quite straight-forwardly since it has previously been done by Bang and Hansteen[17] and Choi and Merzbacher.[22] Computationally, however, such an evaluation is quite involved and BBL make some approximations. In all, four approximations are made:

1) They replace $\omega_{1s\sigma}(R(t))$ by $\omega_{1s\sigma}(R_0)$.

2) Potential coupling is assumed and SA wavefunctions are used in calculating the matrix elements.

3) They use Huus' approximation, valid for $4(v_1/v_K)^2 << 1$, monopole excitations (LM = 00) only, and straight-line trajectories to calculate the cross section.

4) They make various expansions around the SA energy gap.

We elaborate on the latter two of these approximations in Appendix D.

BBL find that the cross section can be written as:

$$\sigma_K = \sigma_K^\circ/\delta^9 \tag{D.13}$$

where σ_K° is Huus' approximation to the cross section without a binding correction factor [Eq. (5.6)]. The factor δ is given by

$$\delta = 1 + U_K^{-1} \, 5/2^5 \int_0^\infty x^5 dx \, K_2^2(x) \, \hbar\omega_{1s\sigma}\left(\frac{\hbar v_1 x}{U_K}\right) \tag{D.10}$$

To calculate δ, a knowledge of the $1s\sigma$ energy gap $\hbar\omega_{1s\sigma}$ as a function of the internuclear distance is required. BBL use:

$$\hbar\omega_{1s\sigma}(R) = U_K + \frac{2Z_1}{Z_2^*} U_s y^{-1}\left[1-(1+y)e^{-2y}\right] \tag{D.14}$$

with $y = R/a_K$. The problem with this form is that it does not give the correct UA energy gap at $R = 0$. We argue that a better form is:

$$\hbar\omega_{1s\sigma}(R) = U_K + (U_{UA} - U_K) y^{-1}\left[1-(1+y)e^{-2y}\right] \tag{D.16}$$

where $y = 1.3R/a_K$, a_K is the K shell radius of the heavier-collision partner, and U_K and U_{UA} are experimental binding energies. Using this

expression, δ is given by

$$\delta = 1 + \frac{U_{UA} - U_K}{U_K} g(1.3\xi_K) \tag{D.18}$$

where $\xi_K = 2/\sqrt{\theta_K}\, v_1/v_K$, and g is a function tabulated by BBL. As $v_1/v_K \to 0$, $g \to 1$, and $\delta U_K \to U_{UA}$ so that

$$\sigma_K = \sigma_K^0 \left(\frac{U_K}{U_{UA}}\right)^9 \tag{5.8}$$

In a symmetric collision the binding-energy corrected cross section should lie $4^9 = 2.6 \times 10^5$ lower than the constant SA energy gap cross section. This is in qualitative agreement with Fig. 15.

BBL show that it is possible to modify the more exactly calculated PWBA cross section to account for the δ factor. The PWBA cross section may be written in terms of a universal function $f(\eta_K, \theta_K)$ as previously described in Eq. (2.3):

$$\sigma = \sigma_0/\delta \; F\left(\eta_K/(\theta_K \delta^2)\right) \tag{D.19}$$

where F is proportional to the f function for $\theta_K = 1$ and $\sigma_0 = 8\pi\, Z_1^2/Z_2^{*2}\, a_K^2$. Finally they also show that it is possible to account for the Coulomb deflection of the projectile by multiplying σ by $9E_{10}(\pi/2\; d_0 U_K \delta/\hbar v_1)$ where d_0 is the distance of closest approach in a head-on encounter, and $E_{10}(x)$ is the exponential integral function of order ten.[59]

It is interesting to compare Eq. (D.19) with the UABEA scaling law of Foster *et al.*[57] For $v_1/v_K \ll 1$, $\delta U_K \approx U_{UA}$ and Eq. (D.19) reduces to:

$$\frac{U_{UA} U_K \sigma}{Z_1^2} \sim F\left(\frac{E_1}{\lambda U_{UA}} \times \frac{U_K}{U_{UA}}\right) \tag{5.9}$$

Aside from the difference of one power of U_{UA} on the left-hand side of this equation, the most significant difference between Eq. (5.9) and the UABEA scaling law [Eq. (4.10)] is the factor of U_K/U_{UA} which multiplies $E_1/\lambda U_{UA}$. In other words, δ enters as the square in Eq. (D.19) and not to the first power as Foster *et al*[57] would have it. The δ^2 factor seems reasonable when we see that the η_K factor originates in the oscillatory factor

$$\omega_{1s\sigma}t \sim \frac{\hbar\omega_{1s\sigma}(R_0)R}{\hbar v_1} = \frac{\delta}{2}\sqrt{\frac{\theta_K}{\eta_K}}\,\frac{R}{a_K}$$

In the equation for the amplitude [Eq. (5.7)], there are practically no other factors of η_K in the integrand. It is this factor which enters into the F function, and it is clear that where η_K enters to first order, δ should be second order. Therefore, although the UABEA modification seems logical at first sight, it is probably not mathematically correct.

Most of the work described in this Section and Appendix D follows directly from BBL. Our only modification was to change the form used for the $1s\sigma$ energy gap [Eq. (D.14)] to more closely reproduce the actual dependence of $\omega_{1s\sigma}(R)$ around $R = 0$ for near symmetric collisions. This only changed some constants in the expression for δ [Eq. (D.18)].

Although BBL make at least four approximations in obtaining Eq. (D.18) and (D.19), it is the best theory thus far available for calculating the cross section for ionization of a $1s\sigma$ electron in asymmetric to near-symmetric collisions. My p + H calculations are

limited to just symmetric collisions, and they too are very approximate. Qualitatively we have shown that there is liable to be some agreement between the two calculations; they both predict a very large difference between the constant SA energy gap results and the binding energy corrected results. In the following section we make a quantitative comparison.

5.3 Comparison

Table I compares the 1sσ ionization cross section for p + H encounters calculated with the two models. There is about a factor of five agreement between the Basbas theory (σ_K^{BBL}) and our model calculations (σ_K^M). The Basbas results give a higher cross section at higher velocities. At low velocities, the Coulomb deflection factor becomes more important, the δ factor becomes larger, and their cross sections are lower than the model calculations. My results are very uncertain at low velocities and I have not included them here.

The main difference between the two calculations is in the δ factor. In the BBL calculations, δU_K varies between 1.44 and 1.7 for projectile energies between 2500 and 700 eV. If I were to define a δU_K factor from Fig. 15, it would only vary between 1.75 and 1.9 over that range. This possibly suggests a modification of $g(\xi_K)$ to make it more constant between 700 and 2500 eV. Since my model calculations may themselves be far off from experiment, there is no justification in modifying $g(\xi_K)$ at this time.

The most remarkable aspect of this comparison, though, is not in the differences between the two calculations but in the similarity. These two calculations start with two very different approaches, yet agree within a factor of five in the final results. Compared to the

approximate factor of 10^4 between what "experiment" predicts in Fig. 15 and our model calculations, the factor of five seems practically negligible.

TABLE I. Cross sections for p + H encounters.

E_1 eV	v_1/v_K	δU_K a.u.	Coulomb factor $9E_{10}$	σ_K^{BBL} a.u.	σ_K^M a.u.
200	0.089	1.8	(8.53×10^{-5})	5.3×10^{-13}	--
700	0.167	1.7	0.251	3×10^{-8}	10×10^{-8}
1000	0.2	1.61	0.468	27×10^{-7}	5×10^{-7}
1500	0.244	1.55	0.666	18×10^{-6}	3.5×10^{-6}
2500	0.316	1.44	0.84	21×10^{-5}	4×10^{-5}

Finally, it is of interest to make a comparison with the impact parameter dependence predicted by BBL. Equation (D.1) indicates that P(b) can be written as

$$P(b) = \frac{C\hbar v_1}{2\pi} b^4 \int_{q'}^{\infty} dq\, q^{-4} K_2^2(bq) \tag{5.10}$$

or

$$P(x) \sim x^7 \int_x^{\infty} dx'\, K_2^2(x')\, x'^{-4} \tag{5.11}$$

where $x = bq' = b\left(q_0 + \Delta q(b)\right)$. Normalizing P(x) to unity $\left(\int_0^{\infty} P(x)\, 2\pi x dx = 1\right)$, the quantity can be calculated with errors less than 1% from the formula[89]

$$P(x) = \frac{1}{8}\left(1 + 1.96x + 1.37x^2\right) e^{-2x} \tag{5.12}$$

One can incorporate Coulomb deflection effects into this expression by evaluating Δq at R_0 instead of b:

$$R_0 = \left[\left(\frac{d_0^2}{4b^2} + 1 \right)^{1/2} + \frac{d_0}{2b} \right] b \tag{5.13}$$

Then

$$x = \frac{R_0}{\hbar v_1} \left(U_K + (U_{UA} - U_K) y^{-1} \left[1 - (1+y) e^{-2y} \right] \right) \tag{5.14}$$

with $y = 1.3\ R_0/a_K$. Figure 18 compares this value of P(b) for p + H collisions with our model calculations. The normalization factors are arbitrary in this figure; the curves have been matched in the approximately exponential regions. Two facets are evident:

1) Our model calculations show that P(b) usually bends over and does not continue to rise as b approaches 0.
2) The BBL result does not drop off exponentially at large b.

The second facet is the result of the changing value of Δq with b. Our model calculations indicate that $x \sim R_0\, f\, U_{UA}/\hbar v_1$, where f is a constant around 0.9 at large b. In the BBL model f steadily decreases with b and this is why his curves deviate from a simple exponential.

In conclusion, the binding correction results of BBL[4] nearly reproduce the model calculations for $1s\sigma$ ionization in p + H encounters. The difference is that they use $\omega_{1s\sigma}(R_0) \approx \omega_{1s\sigma}(b)$ instead of a constant that leads to a variable δ factor instead of a near constant δ factor that would better reproduce our model calculations. It also leads to tails in P(b) instead of the simple exponential fall-off of P(b) calculated with a hydrogenic energy gap.

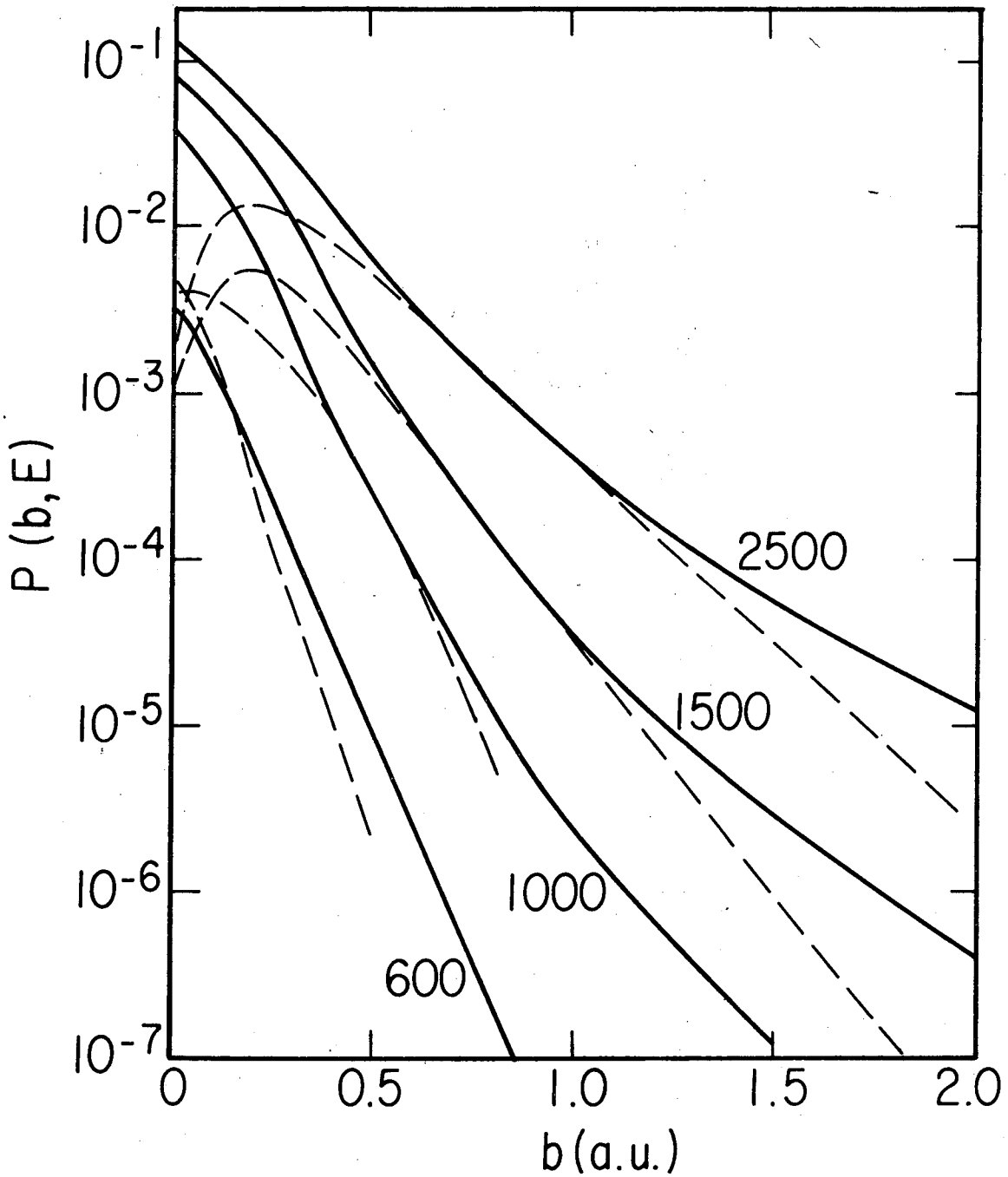

XBL 7512-9772

Fig. 18. The impact parameter dependence of the 1sσ ionization probability P(b,E) versus impact parameter b for 600 - 2500 eV p + H encounters. Dashed line: my model calculations, same as Fig.16. Solid line: BBL results. The curves have been normalized to arbitrary factors.

5.4 Excitation to High, Bound States

The experimentally observed 1sσ cross section comes from both ionization and excitation to high bound states. It is therefore important to find what proportion of the cross section comes from the latter contribution.

Unfortunately, any *ab initio* calculation of the cross section for exciting a 1sσ electron into high bound states must contend with the difficulty that these states are non-adiabatic, i.e., they rarely fulfill the requirement that

$$|\varepsilon_c| > \frac{1}{4}\frac{mE_1}{MA_1} \tag{2.22}$$

For 2500 eV p + H collisions, Eq. (2.22) implies that bound states with binding energy less than 0.34 eV or Rydberg states with $n > 6$ are not well described using adiabatic wavefunctions.

Despite the fact that we cannot directly calculate this cross section using the molecular model, we can make some qualitative remarks about this process and some semi-quantitative estimates of its importance. The first unfilled states in Kr + Kr encounters have principle quantum numbers $n = 5$. The energy transfer required to excite a 1sσ electron into a $n > 5$ Rydberg state is nearly as large as the energy required to ionize the electron, 13.7 versus 14.3 keV. Therefore the qualitative behavior of the excitation cross section and P(b) should be similar to the ionization cross section and P(b). Most importantly, there should be a strong dependence of both quantities on the 1sσ binding energy near the distance of closest approach.

To obtain an estimate of the importance of this cross section, we need only extend the sum over final states to include bound as well

as continuum states. One way of accomplishing this is to replace ε_C in:

$$\sigma(E_1) = \int_{\varepsilon_c}^{\infty} \frac{d\sigma}{d\varepsilon}\, d\varepsilon \tag{5.33}$$

by the (negative) energy of the n = 5 bound state instead of zero as in Eq. (5.2).‡ To evaluate this integral, we used the fact that $d\sigma/d\varepsilon$ drops off as $(U_{UA} + \varepsilon)^{-10}$ (Eq. (5.6) and Fig. 17), and we extrapolated that fit to negative ε energies. The integral Eq. (5.33) is trivial and we obtain as a measure of the importance of the cross section for excitation to high bound states, σ_{HS}:

$$\frac{\sigma_c + \sigma_{HS}}{\sigma_c} \approx \left[\frac{n^2}{n^2 - 0.25}\right]^9 \tag{5.15}$$

where n is the principle quantum number of the first unfilled bound state and σ_C is the cross section for ionization. For n = 5, the contribution from excitation to high bound states is only about 9%. In encounters with highly stripped Kr ions, it may be possible to excite electrons into states as low as n = 2 or n = 3. Even for excitation into n = 3 states, the contribution is only 30%. Excitation into strong coupled n = 2 states should not be considered with this extrapolation. Such excitation occurs via Demkov coupling and $2p\sigma$ excitation which we have already considered. Therefore, as long as excitation to the very lowest bound states can be neglected, it appears that excitation to the high bound states can be neglected in heavy-ion collisions.

This result is not surprising because if this process is important in excitation from molecular orbitals, it should be important in Coulomb

‡Care should be taken about the density of final states and this is discussed in Appendix C. The quoted result is essentially correct though.

excitation from atomic orbitals as well.* Yet all of the light projectile-heavy target work indicates that only ionization is important; at least that is the only process included in the PWBA, SCA, and BEA theories, and they fit the data within a factor of two. Except where degeneracy mediated processes such as rotational transitions to the $2p\pi$ orbital and Demkov transitions predominate, it appears that the neglect of excitation to bound states in heavy ion collisions is even more justified than in the light projectile models.

---

*A similar analysis for light projectile excitation shows that the contribution from high bound state excitation would be slightly greater in that case.

VI. EXPERIMENT AND THEORY

The question that this chapter seeks to answer is: does the 1sσ cross section data display a dependence on the UA energy gap? The first order binding correction results predict that for $g(\xi_K) \sim 1$, δ is approximately U_{UA}/U_K. Therefore, if we bombard one target element with a succession of different projectiles of the same velocity, the cross section should change as:

$$\sigma_K \sim Z_1^2 \, U_{UA}^{-n} \tag{6.1}$$

with $n = 9$. While our model $p + H$ calculations do not indicate how the cross section in asymmetric collisions changes with Z_1, a dependence on the UA energy gap is indicated with n between 5 and 7.

The most useful experiments are those at one projectile velocity, where either the projectile K vacancy cross section is measured as a function of the target atomic number (Z_1 is then interchanged with Z_2 in Eq. (6.1)) or the target K vacancy cross section is measured as a function of Z_1. In this chapter, we shall be using the latter method to obtain the general dependence of n on the induced projectile velocity v_1/v_K.

6.1. The Data

Recently McDaniel and Duggan[60a] reported measurements of target K-vacancy cross sections using a variety of projectiles between H and Cl at energies between 0.5 and 3.0 MeV/a.m.u.. Figure 19 shows some of their cross section data, with σ/Z_1^2 plotted versus the UA binding energy. In the Ti data, the cross section decreases, then rises again. The rise is probably due to Demkov coupling to the 2pσ orbital since the charge

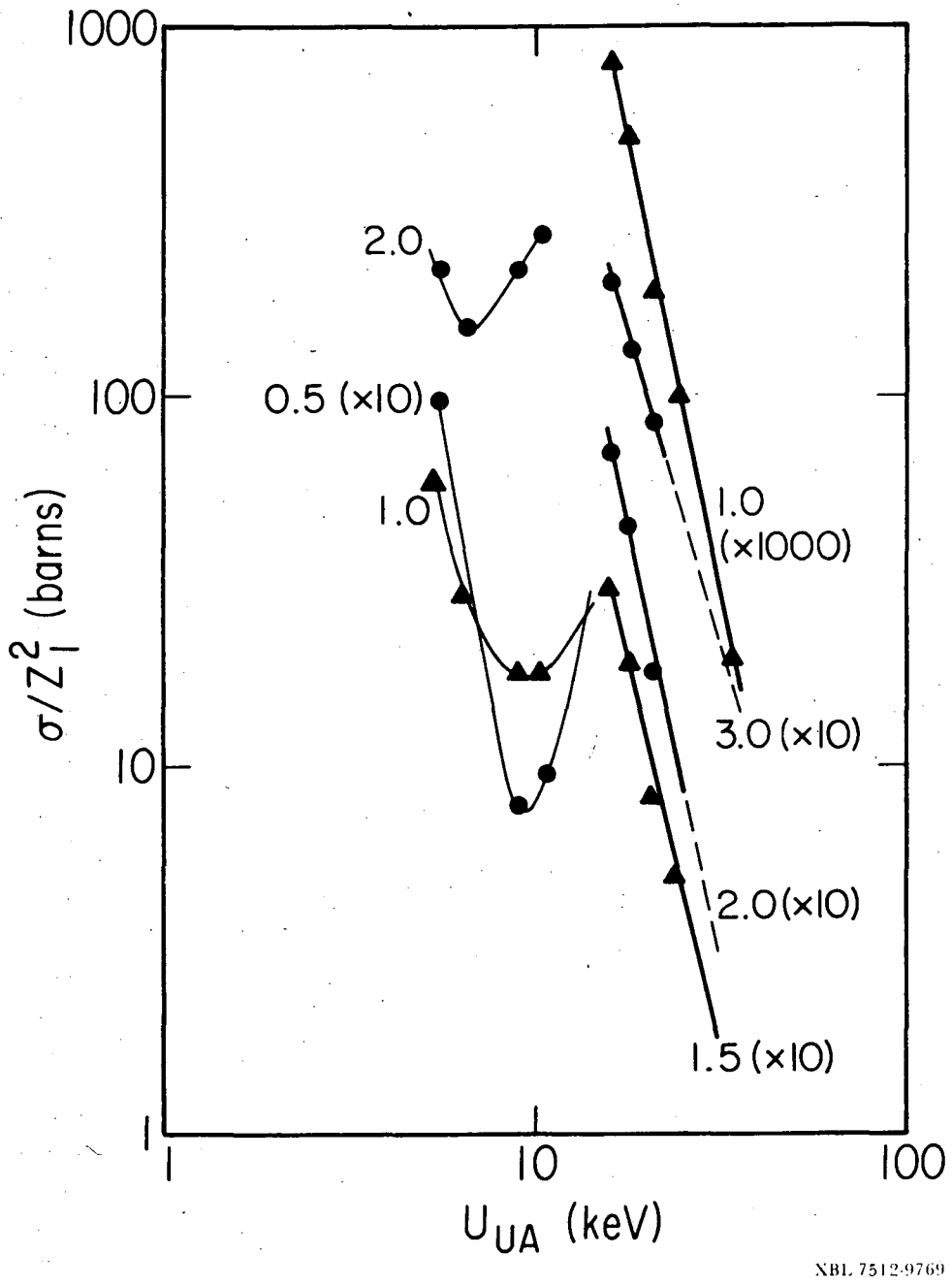

Fig. 19. Target K x ray cross sections for H, He, Li, C, N, O, F, and Cl ions on Ti and Rb. We plot σ/Z_1^2 versus the UA energy gap. Thin line: Ti x ray cross sections for 0.5, 1., and 2. MeV/a.m.u. projectiles. Thick line: Rb x ray cross sections for 1., 1.5, 2., and 2.5 MeV/a.m.u. projectiles.

of the highest-Z projectile in this figure is 17 which is close to the atomic number of Ti. The Rb data, however, displays the expected energy gap dependence given by Eq. (6.1). The slope of these curves changes with projectile velocity giving an n value of 4.8 for 0.5 MeV/a.m.u. to 3.5 for 3.0 MeV/a.m.u..

The data, therefore, does display a dependence on the UA energy gap, but it is not as steep a dependence as theory indicates. To see if this dependence is general, or just in the Rb data of McDaniel and Duggan, we also took other data, plotted σ/Z_1^2 for the same projectile velocity versus the UA energy gap, and extracted n values which are plotted versus v_1/v_K in Fig. 20. Generally, few studies like McDaniel and Duggan's were available and we took scarce oxygen data and measurements using proton or alpha particles. The uncertainty in the individual n values in these figures is plus or minus 0.5 to 1.0.

Figure 20 displays the trend of the n values obtained from this extensive collection of data. At $v_1/v_K \approx 0.1$, n is approximately five. It decreases with larger v_1/v_K, approaching zero at $v_1/v_K \approx 0.5$, then becomes negative indicating that σ/Z_1^2 actually increases with the UA energy gap (or increases with Z_1).

It appears that our expectations of the magnitude of n, or of the steepness of the dependence of the cross sections on the UA energy gap are never fully realized. To obtain the theoretical values of n plotted in Fig. 20, we have used several different approaches:

1) *Binding Correction 1:* In the spirit of the approximation made in writing Eq. (D.9), we write

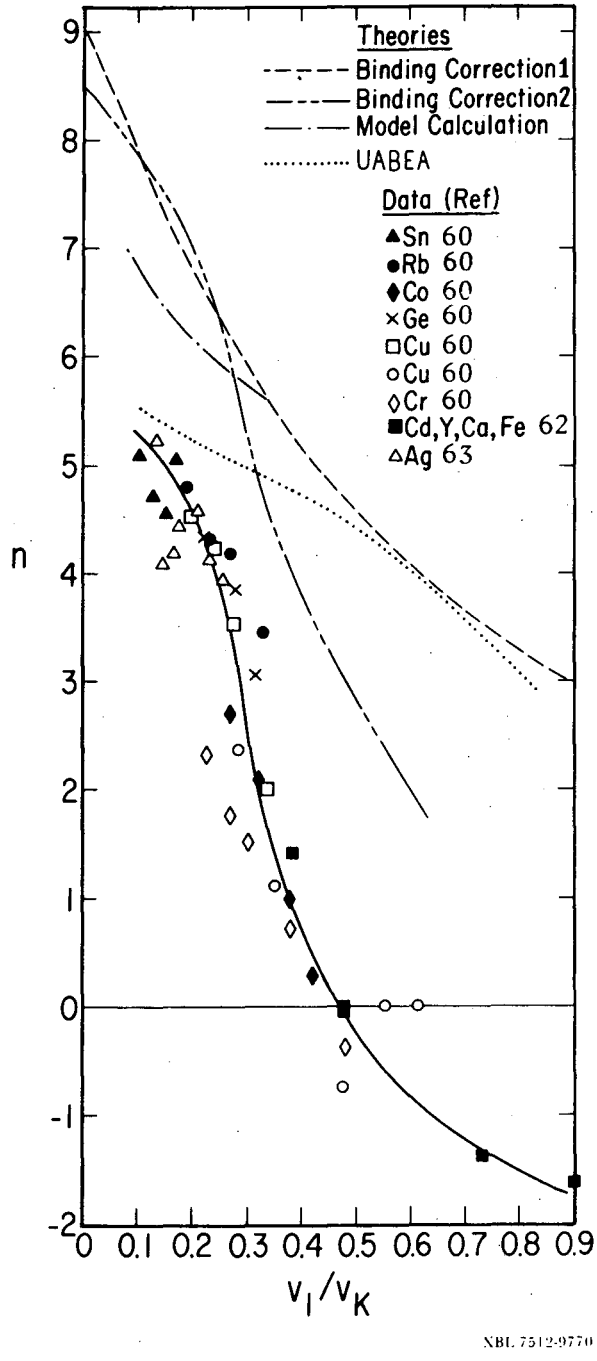

Fig. 20. Heavy ion (generally O) and proton cross sections were used to fit the cross sections to the form $\sigma/Z_I^2 \sim U_{UA}^{-n}$. The value of n is plotted versus v_I/v_K. The proton data was taken from tabulations.[61] The references refer to the source of the heavy ion data. The "theoretical" curves are based on approaches 1-4 described in text.

$$\frac{\sigma_K}{Z_1^2} \sim \left[1 - 9\left(\frac{u_{uA} - u_K}{u_K}\right) g(\xi_K)\right] \approx \left[1 + \frac{u_{uA} - u_K}{u_K}\right]^{-9g} \sim u_{uA}^{-9g} \tag{6.2}$$

hence n is simply $9g(\xi_K)$. Although g is a function of both v_1/v_K and θ_K, the dependence of θ_K can be neglected. We take $\theta_K = 1$ in Fig. 20.

2) *Binding Correction 2:* Neglecting the Coulomb deflection factor, Eq. (D.20) gives

$$\frac{\sigma_K}{Z_1^2} \sim F(\eta_K/\delta^2\theta_K)/\delta \tag{6.3}$$

We constrain the cross section to have the dependence illustrated in Eq. (6.1) so that n can be defined by

$$n = -\frac{u_{uA}}{\sigma}\frac{d\sigma}{du_{uA}} \tag{6.4}$$

Defining $y = \eta_K/\delta^2\varepsilon_K$, n is

$$n = \frac{\delta - 1 + g}{\delta}\left(1 + \frac{2y}{F}\frac{dF}{dy}\right) \tag{6.5}$$

As $v_1/v_K \to 0$, $F \sim y^{3.6}$, and $g \to 1$, therefore $n \to 8.2$. For other velocities, a unique dependence of n on v_1/v_K cannot be defined. We took $Z_1/Z_2 = 0.25$ which is typical for the oxygen data used in Fig. 20. Again, θ_K was taken as unity, but η_K was defined by the experimental binding energy consistent with the horizontal scale in this figure.

3) *Model Calculations:* We took the constant energy gap cross sections displayed in Fig. 15 and plotted cross sections for the same projectile velocity versus the energy gap on a fully logarithmic plot. Values of n were found by measuring the slope of those curves.

4) *UABEA Results:* We took the semi-empirical UABEA scaling law and used Eq. (6.4) to obtain n:

$$n = 2 + \frac{dF}{dx} \cdot \frac{x}{F} \tag{6.6}$$

where $x = E_1/(\lambda U_{UA})$, and F was taken from ref. 1. This value of n is not a unique function of v_1/v_K either since x depends on the UA energy gap instead of the SA energy gap. We again used $Z_1/Z_2 = 0.25$ to evaluate n.

None of the theoretical values of n come close to fitting the data. The prediction of the UABEA scaling law comes closest, but there is no theoretical reason why that particular choice works so well. The theoretical predictions all give values of n that are too high, and none predict that n should become negative for $v_1/v_K > 0.5$. (We shall discuss the negative values of n in the following section.)

The disagreement with the Basbas predictions is not a new result. It has been known for some time that their binding correction over-corrects the data, i.e., it gives cross sections for heavy ions that are much lower than experiment. For instance, McDaniel and Duggan show that it fails to predict the Rb ($Z_2 = 37$) K x ray cross sections in encounters with $7 < Z_2 < 17$. My modification to the BBL theory would mean that the correction factor would be larger, hence the disagreement would be worse.

6.2. Other Corrections

One possible reason why the data never displays a UA energy gap dependence as large as theory indicates is that there are other contributions to the 1sσ cross section which increase σ/Z_1^2 with Z_1 or the UA energy gap. Three such contributions have been discussed in the literature. They are polarization effects, charge exchange between the target and projectile K shells, and the Demkov effect. These three are discussed in this section. Aside from the Coulomb deflection and binding correction effects which give negative contributions to σ/Z_1^2, there are no other Z_1 contributions to the 1sσ cross section that could affect the data in question.†

6.2.1 Polarization

In collisions with projectile velocities $v_1 > v_K$, the "radius of excitation" [see Eq. (5.3)] becomes greater than a_K. The K-shell orbits are distorted by the field of the projectile, $\mathcal{E} \lesssim Z_1 e^2/a_K^2$, by a relative amount $\delta/a_K = \alpha\mathcal{E}/a_K e$ where α is the K-shell polarizability. The interaction distance is thus shortened, increasing the strength of the interaction between the projectile and the K-electron, giving an additive contribution to the 1sσ cross section.

The only theoretical treatment of the polarization effect was originally formulated to consider Z_1^3 contributions to stopping power formulas.[77] The treatment is somewhat stylized; the bound K-electron is considered as a harmonic oscillator whose motion is displaced by the

---

†At relativistic projectile energies a positive Z_1^3 term is known.[33] Its importance requires that $v_1/v_K \gg 1$ and $\beta = v_1/c \approx 1$.

projectile's Coulomb field. The oscillator absorbs energy from the projectile's motion through a sort of virtual photon interaction, reminiscent of the Weizsäcker-Williams approach.[78] Basbas *et al*[2] have applied the stopping power results to the problem of K-vacancy production. The cross section can be written as:

$$\sigma = \sigma_0 \left[1 + \frac{Z_1}{Z_2} \left(\frac{v_1}{v_K} \right)^3 \int_{u_K}^{\infty} g_K(\omega)\, I\left(\frac{\omega a_K}{v_1} \right) \frac{d(\hbar\omega)}{F(\eta_K)} \right] \tag{6.7}$$

where σ_0 may be considered as first order PWBA or SCA cross section, and F is the universal function similar to that defined in Eq. (D.19). The function $g(\omega)$ is the differential oscillator strength distribution normalized to $\int_0^\infty g(\omega)d\omega = 1$, and $I(\omega a_K/v_1)Z_1^3$ is proportional to the integral of the Z_1^3 correction to the classical energy transfer over impact parameters $b > a_K$. Another way of viewing this result is that I is proportional to part of the intensity of the virtual photon field of the projectile,[‡78] and $g(\omega)$ is proportional to the probability that the K-electron will absorb photons from the virtual field and be ejected to the continuum.

Most of the work in this thesis is based on the molecular model and it is valuable to discuss the polarization effect in light of this model. Unfortunately, the polarization effect is important at velocities

---

‡The virtual photon field $I(\omega)$ is proportional to the square of the Fourier transform of the time dependent electric field $\vec{E}(t)$ averaged over impact parameters. The electric field depends on the instantaneous distance between the electron at $\vec{r}_0(t)$ and the projectile at $\vec{R}(t)$. The electron motion is polarized so that its position is changed by an amount $\vec{\Delta r}(t)$. The electric field is expanded about $\vec{r}_0(t)$ and can be written as $\vec{E}(t) = \vec{E}_0(t) + \Delta\vec{E}(t)$. The $\Delta\vec{E}(t)$ term gives a ΔI term upon squaring the Fourier transform of $\vec{E}(t)$, and it is the ΔI term which is in Eq. (6.7).

where the molecular model starts to break down, namely when $0.5 < v_1/v_K < 1$. While the wavefunctions of the projectile and target are still expected to form MOs in this region ($v_1/v_K < 1$), other concepts such as the classification of processes into energy transfer and degeneracy mediated processes have already broken down. The oscillatory parts of the amplitudes are no longer as highly oscillatory, hence the energy gap loses its importance in this region. I also suspect that the UA energy gap will no longer be important and the n dependence of the UA energy gap may approach zero quite quickly. Finally, in certain cases the SCA method used for calculating the binding correction also breaks down.

The theory of the polarization effect rightfully recognizes that it is not the effect of the molecular energy levels that will be important here, but the effect of the molecular wavefunctions. It is assumed that the electronic motion is changed by the projectile; the electrons move in MOs where part of the electronic density is shifted closer to the projectile. In the SCA or PSS picture, this will mean a change in the matrix elements.

In contemplating a better calculation of the polarization effect, one problem is that the PSS method may no longer be valid. The SCA upon which the method of PSS is based, requires that the Sommerfeld parameter[17] be much greater than unity:

$$\chi = 2Z_1Z_2e^2/\hbar v_1 = 2Z_1v_K/v_1 \gg 1 \qquad (6.8)$$

Unfortunately, for light projectiles at $v_1/v_K > 1$, the SCA and the PSS method will no longer be valid.

For this reason, we shall use estimates based on Eq. (6.7) to evaluate the importance of polarization effects. Some estimates are

given in Figs. 21 and 22. Figure 21 was taken from McDaniel and Duggan,*[60a] and shows the importance of the polarization terms for Li, C, and N ion induced K-vacancy production in Ti. The polarization term gives a substantial additive contribution to the cross section for $v_1/v_K > 0.5$. The contribution becomes steadily smaller for smaller values of v_1/v_K, however, and therefore is not likely to make a large change in n at $v_1/v_K \sim 0.1$. Hence, the polarization contribution does not appear to explain why n is so much smaller than the theoretical estimates at very low velocities.

The second figure is taken from Basbas *et al*[2] and illustrates the importance of the polarization term at larger values of v_1/v_K. This plot is similar in many respects to our n plot. The ratio He to H induced cross sections (divided by four) becomes greater than unity at approximately $v_1/v_K = 0.5$ or ½, similarly n becomes negative at approximately 0.5. When $v_1/v_K \gg 1.0$, Eq. (6.7) adequately explains the ratio R_{2K}. For the very light ions used in this work, the binding energy and Coulomb deflection contributions explain R_{2K} for $v_1/v_K \lesssim 0.1$. Unfortunately, He to H cross section ratios do not provide as good a test of the binding correction term as Cl to H or O to H ratios. Our n plot is a more sensitive test of the binding correction.

Finally, I should note that the polarization correction does not scale strictly with the UA energy, but instead σ/Z_1^2 is linear in Z_1. Although we observe negative values of n in Fig. 20 which we attribute to polarization, the fit of the polarization affected data to the U_{UA}^{-n} dependence is not strictly justified.

---

*No details of the evaluation of this term was given in McDaniel and Duggan's paper. I have assumed that this figure is based on Eq. (6.7).

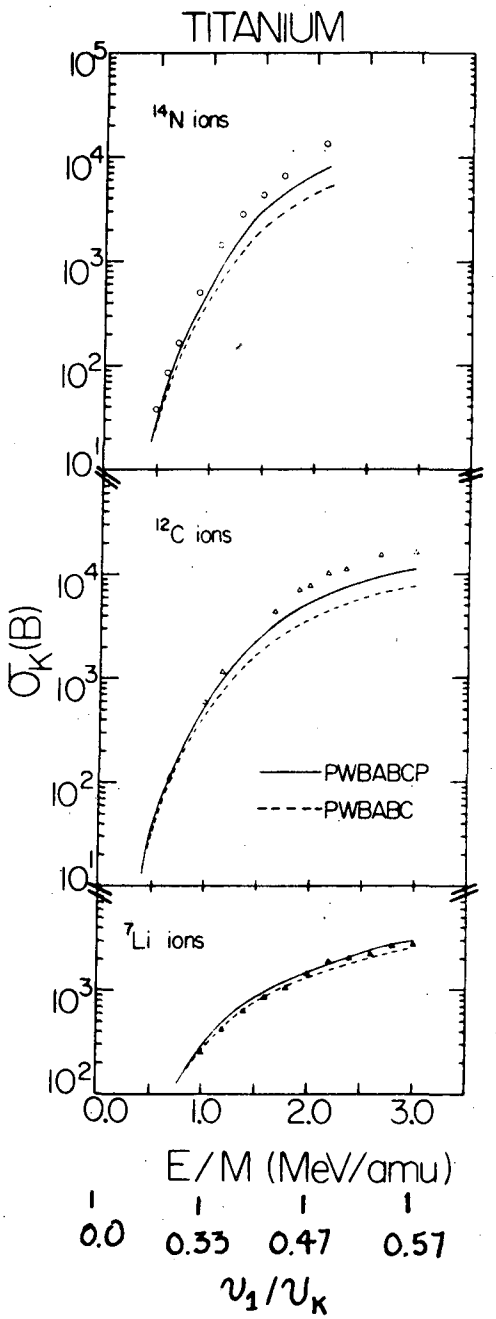

Fig. 21. Ti x ray cross sections for incident Li, C, and N ions. Theoretical curves are presented for binding corrected PWBA cross sections (PWBABC, using the original method of BBL), and corrections for binding + polarization terms (PWBABCP); from Ref. 60a.

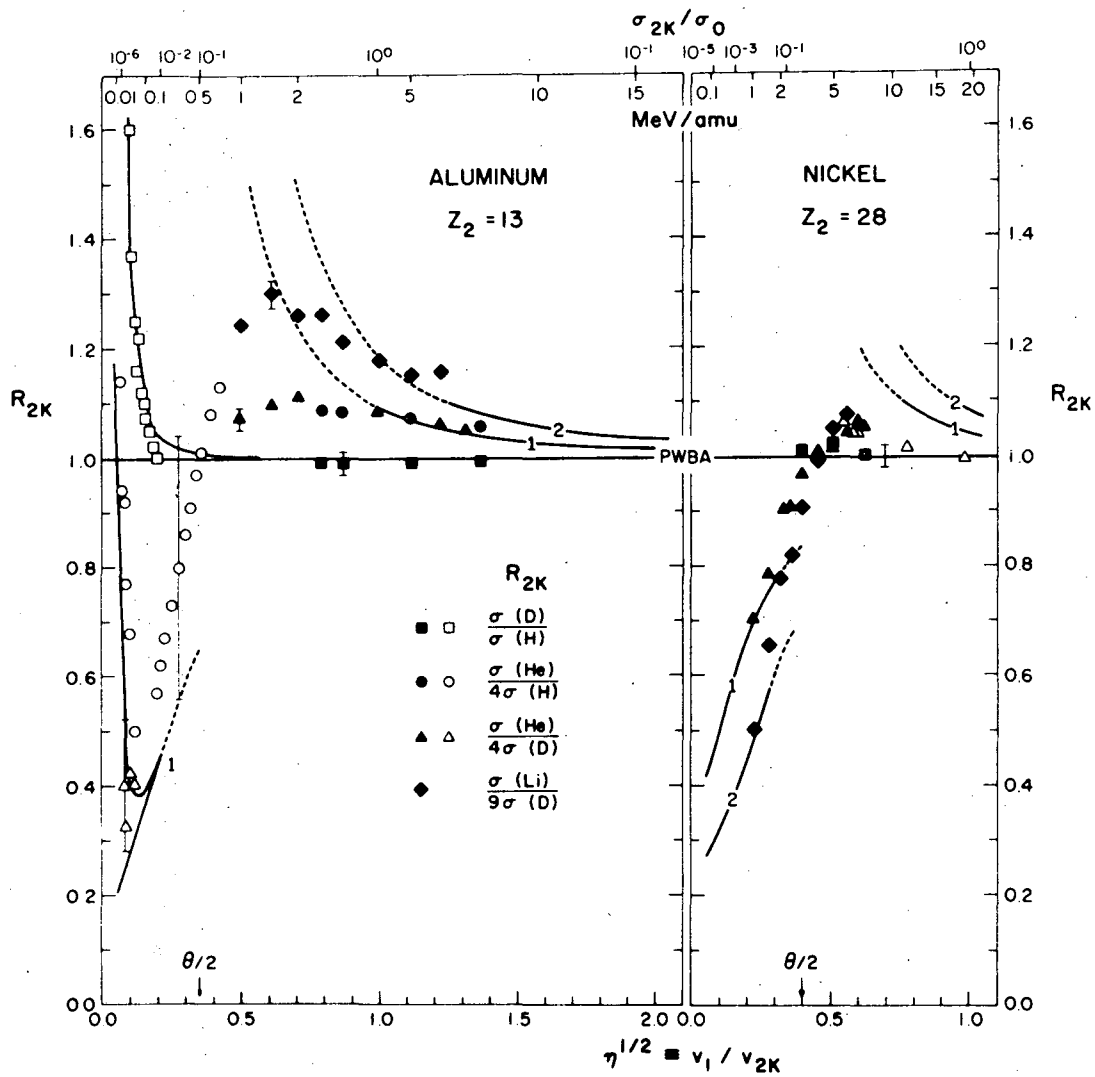

Fig. 22. Ratios of He induced to H induced Al and Ni K x ray cross sections divided by four as a function of v_1/v_K. The upper scale gives the particle kinetic energy in MeV/a.m.u. and a nomograph of the ionization cross sections for Z = 1 in units of $\sigma = 8\pi Z_1^2/Z_2^2 a_K^2$. For large v_1/v_K, the curves show the contribution from the polarization term. For small v_1/v_K they show the binding term (from ref. 2).

6.2.2 Charge exchange and Demkov coupling

Both of these processes are charge exchange phenomena. With the former, we mean charge exchange from the target K-shell to an empty projectile K-shell such as would occur when fully stripped projectiles bombard target atoms differing in Z by not more than ten.[79,80] Demkov coupling,[30,31] though, is charge exchange between the 2pσ and 1sσ MOs (or conceivably, between any two MOs). Usually, it is operative in encounters at low velocities where the projectile K-shell is not empty and correlates to the 2pσ orbital ($Z_1/Z_2 < 1$). Vacancies are made in the 2pσ orbital during the collision and are exchanged for 1sσ or target K-electrons on the outgoing part of the collision. We have discussed this process previously.

The charge exchange process complements the Demkov process. The criterion as to which is important must be the magnitude of v_1/v_{K1} where v_{K1} is the velocity of the electron in the K-shell of the projectile.† This criterion not only decides whether MOs (especially the 2pσ MO) will be formed, but it is also the Bohr criterion[81] for completely stripping the projectile. When $v_1/v_{K1} > 1$, the projectile K-shell is unfilled, MOs will probably not be formed, and charge exchange between atomic orbitals will occur. Usually, the Brinkman-Kramers[79,82] or BEA formulas[80] are used to calculate these cross sections. When $v_1/v_{K1} << 1$, MOs will be formed, the projectile K-shell will normally be full, and the Demkov process will predominate.

For example, if one bombards Ti with ions with $Z_1 < 22$ and $E_1 = 3$

---

†This argument is valid when target x rays are measured as a function of Z_1, where $Z_1 < Z_2$.

MeV/a.m.u., it is expected that charge exchange should give a positive contribution to the Ti K cross section up to $Z_1 = 13$ where $v_1/v_{K1} = 1$. For higher Z_1, the Demkov effect is expected to add to the cross section giving the rise observed in Fig. 19. For the same range of projectiles on Rb, however, the charge exchange effect will again be operative up to $Z_1 = 13$, but the Demkov effect should not become important until $Z_1 = 17$. If the charge exchange effect were important one would observe deviations from the straight lines in Fig. 19 up to $Z_1 = 13$, then the data should bend back toward the line up to $Z_1 = 17$. This is not observed though.

Specific instances where charge exchange effects may be an important contributor to the value of n may be seen in Fig. 20. Fully stripped oxygen (before entering the target or immediately thereafter) data was used to obtain the Co, Ge, and Cu cross sections and hence charge exchange may affect the value of n in those cases. In the data of Cue *et al*[62] (Cd, Y, Ca, and Fe points), only very high-energy fully stripped projectiles were used. In those cases, though, the authors concluded that the contribution from charge exchange was small and attributed the deviations from Z_1^2 scaling to polarization and the binding correction term. Finally, it is unlikely that these charge exchange corrections affect the Sn, Ag, and Rb data. Polarization is also not as important for those cases since, coincidentally, $v_1/v_K \ll 1$. The values of n there must be due mostly to the binding energy correction. It appears that none of the positive Z_1^3 contributors to the $1s\sigma$ cross section discussed in this chapter explain the low values of n displayed in Fig. 20.

6.3 Conclusions

The $n(v_1/v_K)$ plot displayed in Fig. 20 provides a useful focus in discussing the behavior of the $1s\sigma$ cross section due to binding correction, Coulomb deflection, charge exchange, and polarization effects. Probably, for $v_1/v_K \gtrsim 0.1$, the most important effects come from the binding correction and polarization terms. For $v_1/v_K < 0.5$, the binding effect is most important and positive values of n are achieved. For $v_1/v_K > 0.5$, polarization effects are more important and n is negative. At $v_1/v_K \approx 0.5$, the two effects cancel. Charge exchange effects (including Demkov) are expected to be important only if $Z_1 \approx Z_2$, but for the most part appear to be negligible. Coulomb deflection is expected to be important for $v_1/v_K < 0.1$, but we include no data for that region in Fig. 20. The various effects discussed in this chapter are summarized in Table II.

Finally, the n plot also provides a test of scaling laws. For instance, the UABEA scaling law[57] comes closest to predicting the correct dependence of n on v_1/v_K. The BBL binding correction, though not strictly speaking of a scaling law, does not do as well. Meyerhof's $1s\sigma$ scaling law cannot be plotted here; it predicts a SA energy gap dependence hence we would expect $n = 0$.[‡] In conclusion therefore, Fig. 20 indicates that while no scaling law dependence best fits the experimental dependence of the cross sections on UA energy, the UABEA law comes closest of all of them.

[‡]Actually, the Z factors in Eq. (4.9) contribute to a UA energy gap dependence. They predict that $n < 0$, however.

TABLE II.

"Effects"	Theory	Sign of Z_1^3 contribution
	$v_1/v_K < 1$	
Coulomb deflection	SCA[17]	-
Molecular	Binding correction. Excitation out of 1sσ orbital. PSS method.	-
Charge exchange	Projectile K-shell full. Forms 2pσ MO Demkov effect. PSS method.	+
	$v_1/v_K > 1$	
Coulomb deflection	SCA no longer valid for light projectiles. Effect probably not important	-
Molecular	Polarization effect. PSS method no longer valid.	+
Charge exchange	Projectile K-shell empty. No MOs formed. Brinkman-Kramers, Born, or BEA theories of charge exchange. v_K is v_{K1}.	+

VII. CONCLUSIONS

Let us examine heavy ion data where the projectile is the higher-Z collision partner. Figure 23 shows projectile K-vacancy cross sections for 200 MeV Kr, 326 MeV Xe, 30 MeV Br, and 47 MeV I ions on targets with $Z_1 > Z_2$. To obtain cross section data from thick target yields, Eq. (3.5) was used. The cross sections are accurate to about 40%.*

The theoretical curves compare the cross section obtained using the BBL binding correction (with my UA modification), the UABEA scaling law prediction,[57] and a completely empirical prediction which uses Eq. (6.1) with values of n taken from the n plot. The curve is normalized using the experimental $p + Z_1$ cross section. Table III gives the proton cross section[61] together with values of n used. The uncertainty in the derived $Z_1 + Ne$ cross section due to the uncertainty in the n value is also given.

TABLE III. Cross sections

Z_1	E_1 MeV/amu	σ_{H^+} barns	v_1/v_K	n	σ_{Ne} barns
36	2.4	35	.30	3.7 ± 0.5	609 ± 150
54	2.4	0.5	.194	4.5 ± 0.5	11.2 ± 2.2
35	0.375	0.065	.123	5.4 ± 0.5	0.476 ± .12
53	0.37	4×10^{-4}	.078	5.6 ± 0.5	$(60.4 \pm 20) \times 10^{-4}$

*The Xe measurements are from a very recent experiment and the results are preliminary.

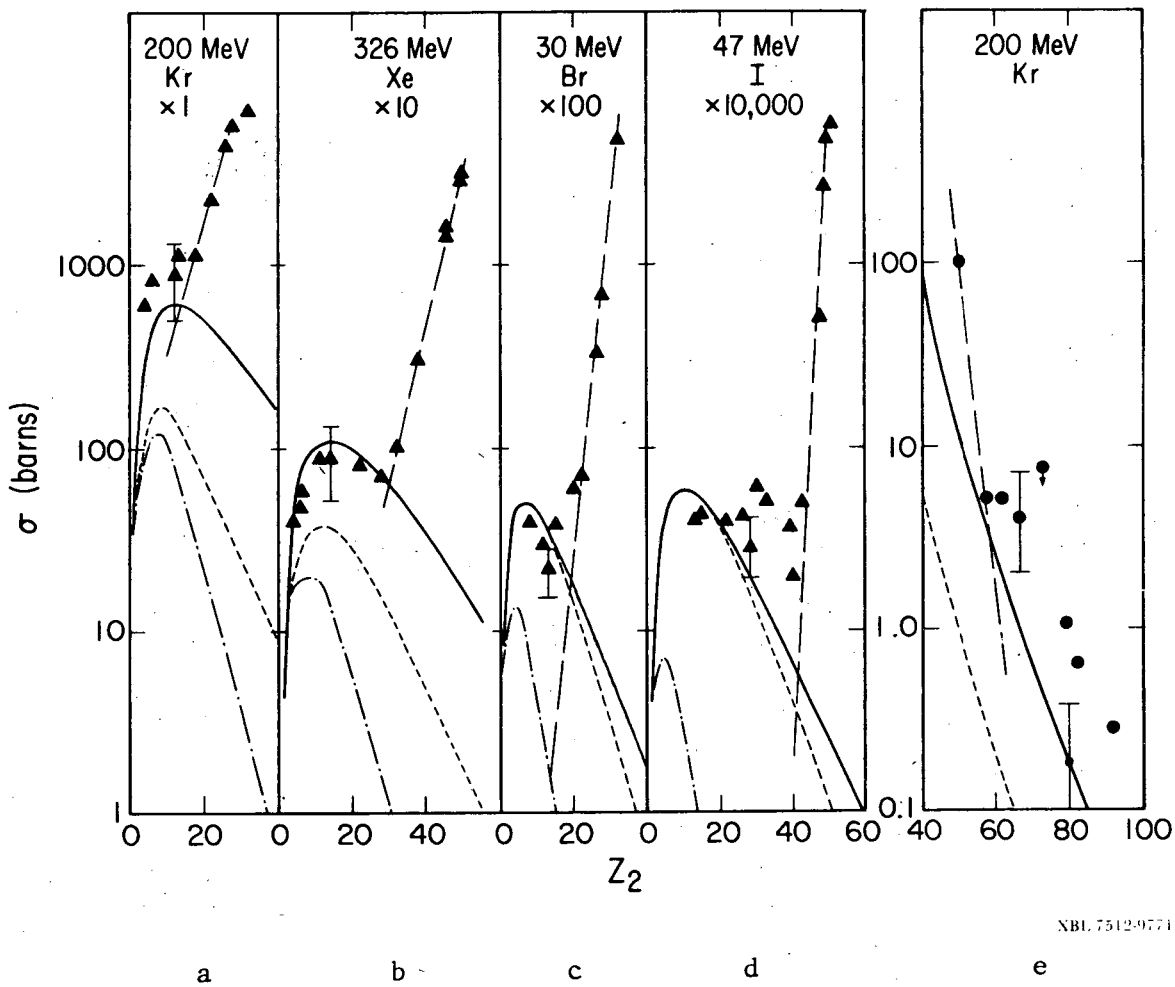

Fig. 23 (a - d): Projectile K vacancy cross sections for 200 MeV Kr, 326 MeV Xe, 30 MeV Br, and 47 MeV I ions incident on target atoms with $Z_1 < Z_2$. Figure 23(e): Target K vacancy cross sections for 200 MeV Kr ions. Long dashed line: Demkov contribution from 2pσ excitation. Solid line based on n plot and Eq. (6.1). Short dashed line: UABEA scaling law. Dash-dot: BBL binding correction.

Several conclusions can be drawn. First, the empirically predicted cross section based on the $p + Z_1$ ionization cross section† is in good agreement with the data. This supports the conclusion that we are observing $1s\sigma$ ionization when we measure projectile K-vacancy cross sections where $Z_1 \gtrsim 2Z_2$. The Kr cross sections are higher than they should be, and this is probably because there is a sizeable contribution from Demkov feeding of $2p\sigma$ vacancies to the projectile in that case. The fit to the Xe cross sections is very good as is the fit to the 30 MeV Br data as near as we can tell. There is clearly insufficient data in the Br case. In the I data, there is a region between $Z_2 = 30$ and 40 where the cross section is not explained by either Demkov feeding or $1s\sigma$ ionization. We have no explanation for this observation. It could mean that either n is much smaller than our curve predicts, or Eq. (6.1) is breaking down, or the Demkov contribution is greater than we think there. No conclusions about this region can be made at this time.

Secondly, it appears that the best scaling law available is our n plot. The BBL binding correction does not do well at all. The UABEA law[57] does as well as our empirical method for the Br and I data, but fails to predict the Xe and Kr cross sections. The reason for this can be seen by examining the n plot. The UABEA law gives nearly the experimental n value at low v_1/v_K ($v_1/v_K \sim 0.1$ in the Br and I cases), but gives an n value which is much too high at larger v_1/v_K (the Xe and Kr cases). Probably the reason why our n plot works so well in these

---

†Plus excitation to high, bound states which is expected to be negligible.

cases is because in deriving n, we used mostly target K-vacancy cross sections around the same atomic number as Br, Kr, I, and Xe. Our n plot may not represent a universal curve; there may be a family of curves with different n dependences for different values of the SA binding energy, Z_1/Z_2, of some other parameter. So far the data cannot distinguish this though.

Using our n plot and K-vacancy production cross sections for 2.4 MeV protons, we have tried to predict target K-vacancy cross sections for 200 MeV Kr encounters with target atoms with $Z_2 > 40$. These predictions are shown in Fig. 23e. The n plot does not do well in these cases, but does do better than the UABEA scaling law. Possibly, the reason why our n plot fails to predict the 1sσ cross sections in these cases is because relativistic effects are becoming important for these high-Z elements. Relativistic effects on high-Z K vacancy cross sections have been noted in the literature.[83-87] The importance of these effects can be understood classically when we try to calculate the minimum initial electron kinetic energy E_2 needed to give an energy transfer U_K [see Eq. (2.10)]. We find that $E_2 > 255$ keV, or that the electron must be moving at relativistic velocities. K-vacancy cross sections have been calculated using Dirac wavefunctions and the SCA and PWBA theories.[83,84] Theory and experiment[26,85-87] agree that these relativistic effects make the K-vacancy cross section larger than non-relativistically calculated cross sections. In Fig. 23 these relativistic effects have already been partly incorporated because experimental proton cross sections were used. Probably, though, there is some effect on the n values as well and that may be the reason why our empirical predictions of these cross section fail.

There is one question left unanswered. We have shown that the positive contributions to the 1sσ ionization cross sections due to polarization effects should be small for $v_1/v_K \lesssim 0.2$. Also, we can show that charge exchange effects and Demkov coupling do not make a great contribution to the cross section in most cases, for instance in the Xe and I data for $Z_2 < 30$ and in the Br data for $Z_2 < 20$. Yet in those cases where $v_1/v_K \lesssim 0.2$, the dependence of the cross sections on the UA energy gap is never as great as theory leads us to expect. The BBL binding correction implies that $n \approx 9$ for $v_1/v_K < 0.2$. Our model calculations imply that n lies between 6 and 7. Yet the data indicates that n never exceeds 5.5.

There are good reasons to expect that these two theories are wrong. While the BBL binding energy correction and the model PSS calculations had their usefulness in pointing out the dependence of the cross sections on the UA energy gap, the magnitude of that dependence may not be accurately predicted by either of them. The BBL theory is based on four approximations including the expansion of the cross sections around the SA binding energy assuming the difference between the SA and UA energy gaps is small. Asymptotically $(g(\xi_K) \to 1)$ the correct physical result was obtained, but it is doubtful whether the function $g(\xi_K)$ is very accurate. My model calculations illustrate the qualitative behavior of the cross section, but the magnitude of those cross sections can certainly not be trusted. Those calculations are extremely sensitive to the functional dependence chosen to fit the matrix elements (see Appendix B) and there is no guarantee that the simple exponential function is best. Clearly, more exact PSS calculations of the 1sσ ionization cross section are still needed before these empirical values of n can be predicted.

REFERENCES

1. J. D. Garcia, R. J. Fortner and T. M. Kavanagh, Rev. Mod. Phys. 45, 111 (1973).
2. G. Basbas, W. Brandt, R. Laubert, A. Ratkowski and A. Schwarzschild, Phys. Rev. Lett. 27, 171 (1971); and G. Basbas, W. Brandt and R. Laubert, Phys. Lett. 34A, 277 (1971).
3. R. Anholt, TOSABE Group, manuscript in preparation.
4. G. Basbas, W. Brandt and R. Ritchie, Phys. Rev. A7, 1971 (1973).
5. J. H. McGuire, Phys. Rev. A8, 2760 (1973).
6. E. Merzbacher, Quantum Mechanics (John Wiley: New York, 1970).
7. W. Lichten, Phys. Rev. 164, 131 (1967); M. Barat and W. Lichten, Phys. Rev. A6, 211 (1972).
8. S. Sackmann, H. O. Lutz and J. Briggs, Phys. Rev. Lett. 32, 805 (1974).
9. J. S. Briggs and J. H. Macek, J. Phys. B: Atom-Molec. Phys. 6, 982 (1973), 6, 841 (1973), and 5, 579 (1972).
10. W. E. Meyerhof, T. K. Saylor, S. M. Lazarus, A. Little and R. Anholt, to be published.
11. Q. C. Kessel and B. Fastrup, Case Studies in Atomic Physics (North-Holland: Amsterdam, 1973) 3, 137.
12. B. Fastrup, invited talk IX ICPEAC.*
13. D. H. Madison and E. Merzbacher, "Theory of Charged Particle Excitation", in Atomic Inner-Shell Processes (B. Craseman, ed) (Academic Press, 1975).
14. E. Merzbacher and H. W. Lewis, Handbuch der Physik (Springer-Verlag: Berlin, 1958) 34, 166.
15. J. D. Garcia, Phys. Rev. A1, 280 (1970).
16. J. H. McGuire, P. Richard, Phys. Rev. A8, 1374 (1973).
17. J. Bang and J. M. Hansteen, Kgl. Danske. Videnskab. Selskab. Mat-Fys. Medd. 31, #13 (1959).
18. N. F. Mott and H. S. W. Massey, The Theory of Atomic Collisions, third edition (Clarendon Press, Oxford, 1965).
19. W. R. Thorson, J. Chem. Phys. 42, 3878 (1965), Phys. Rev. 181, 230 (1969); Hiram Levy II and W. R. Thorson, Phys. Rev. 181, 244 (1969); Phys. Rev. 181, 252 (1969); C. F. Lebeda, W. R.

Thorson, Hiram Levy II, Phys. Rev. A4, 900 (1971); V. SethuRaman, W. R. Thorson and C. F. Lebeda, Phys. Rev. A8, 1316 (1973).

20. J. C. Slater, Phys. Rev. 36, 57 (1930).
21. B. H. Choi, G. S. Khandelwal and E. Merzbacher, Atomic Data 1, 103 (1969).
22. B. H. Choi and E. Merzbacher, Phys. Rev. 177, 233 (1969).
23. J. M. Hansteen, O. M. Johnsen, L. Kochbach, Atomic and Nuclear Data 15, 305 (1975).
24. E. Gerjuoy, Phys. Rev. 148, 54 (1966).
25. L. Vriens, "Binary Encounter and Classical Collision Theories", in Case Studies Atomic Physics, ed. E. W. McDaniel and M. R. C. McDowell (North-Holland: Amsterdam, 1969).
26. J. S. Hansen, Phys. Rev. A8, 822 (1973).
27. E. Laegsgaard, J. V. Anderson and L. C. Feldman, Phys. Rev. Lett. 29, 1206 (1972).
28. J. S. Briggs, preprint (1975).
29. L. Landau, Z. Sowjetunion 2, 46 (1932); and C. Zener, Proc. Roy. Soc. (London) A137, 696 (1932).
30. Yu. N. Demkov, Soviet Phys. JETP 18, 138 (1964).
31. W. E. Meyerhof, Phys. Rev. Lett. 31, 1341 (1973).
32. W. R. Thorson, J. Chem. Phys. 42, 3878 (1965).
33. J. Eichler and U. Willie, Phys. Rev. Letters 33, 56 (1974).
34. D. R. Bates, D. Sprevak, J. Phys. B4, L47 (1971) .
35. S. B. Schneiderman and A. Russek, Phys. Rev. 181, 311 (1969).
36. W. R. Thorson, private communication (July 1975).
37. J. S. Briggs, "Theory of Inner-Shell Excitation in Slow Ion-Atom Collisions", invited talk, IX ICPEAC*(1975).
38. K. Taulberg, J. Vaaben, Abstracts, IX ICPEAC*(1975), p. 1054.
39. H. Kubo, F. C. Jundt, K. H. Purser, Phys. Rev. Lett. 31, 674 (1973).
40. D. A. Landis, C. Jones, B. V. Jarrett, A. Jue and S. D. Wright, unpublished report LBL-540 (1972).
41. J. O. Radeloff, L. B. Robinson, J. D. Meng, unpublished report UCRL-18883 (1969).
42. E. Storm and I. Israel, Nucl. Data A7, 565 (1970).
43. W. H. McMaster, N. Kerr Del Grande, J. H. Mallet, J. H. Hubbel, unpublished report, UCRL-50174, Sec. II, Rev. 1 (1969).

0 0 0 0 4 2 0 0 0 4 3

LEGAL NOTICE

This report was prepared as an account of work sponsored by the United States Government. Neither the United States nor the United States Atomic Energy Commission, nor any of their employees, nor any of their contractors, subcontractors, or their employees, makes any warranty, express or implied, or assumes any legal liability or responsibility for the accuracy, completeness or usefulness of any information, apparatus, product or process disclosed, or represents that its use would not infringe privately owned rights.

TECHNICAL INFORMATION DIVISION
LAWRENCE BERKELEY LABORATORY
UNIVERSITY OF CALIFORNIA
BERKELEY, CALIFORNIA 94720